
**Targeting the hsa_circ_0000253/miR-7/COL5A2 Axis:
Unveiling CCT-018159's Role in Halting Osteosarcoma
Progression**

| | |
|-------------------------------|---|
| Journal: | <i>European Journal of Clinical Investigation</i> |
| Manuscript ID | EJCI-2024-1636 |
| Wiley - Manuscript type: | Original Article |
| Date Submitted by the Author: | 07-Sep-2024 |
| Complete List of Authors: | Guo, Xu; Dalian University of Technology School of Life and Pharmaceutical Sciences Zhu, Xiangrui; Dalian University of Technology School of Life and Pharmaceutical Sciences; Peking University School of Basic Medical Sciences Tian, Xin; Dalian University of Technology School of Life and Pharmaceutical Sciences Dai, Yunfeng; Yingkou Fangda Hospital, Department of Pathology Tsedenbal, Batchimeg; Mongolian National University of Medical Sciences; National Center for Pathology Ibrahim, Mahmoud A.A; Minia University Faculty of Science; University of KwaZulu-Natal School of Health Sciences Han, Yanshuo; Dalian University of Technology School of Life and Pharmaceutical Sciences Liu, Jinzhu; People's Hospital of Shenzhen, Department of Orthopedic Surgery |
| Manuscript Topic: | Basic/Translational |
| Keywords: | Osteosarcoma, circRNA, ceRNA, Cancer Prognosis, Targeted Therapy, Single-cell Transcriptome |
| | |

Title page**1. Title**

Targeting the hsa_circ_0000253/miR-7/COL5A2 Axis: Unveiling CCT-018159's Role in
Halting Osteosarcoma Progression

2. A short running title

hsa_circ_0000253/miR-7/COL5A2 Axis & CCT-018159 in OS

2. Full list of authors and affiliations

Xu Guo, MSc¹#; Xiangrui Zhu, MSc^{1,2}#; Xin Tian, BSc¹; Yunfeng Dai, PhD³; Batchimeg Tsedenbal, PhD^{4,5}; Mahmoud A.A Ibrahim, PhD^{6,7}; Yanshuo Han, MD^{1*}; and Jinzhu Liu, MD^{8*}.

1. School of Life and Pharmaceutical Sciences, Dalian University of Technology, Panjin 124001, China.

2. Department of Physiology and Pathophysiology, School of Basic Medical Sciences, Peking University, Beijing, 100191, China;

3. Department of Pathology, Yingkou Fangda Hospital, Yingkou, 115001, China.

4. Mongolian National University of Medical Sciences, Mongolia.

5. National Center for Pathology, Mongolia.

6. Computational Chemistry Laboratory, Chemistry Department, Faculty of Science, Minia University, Minia 61519, Egypt

7. School of Health Sciences, University of KwaZulu-Natal, Westville Campus, Durban 4000, South Africa

8. Department of Orthopedic Surgery, The Third People's Hospital of Shenzhen, Shenzhen 518000, China.

Contributed equally.

*Corresponding authors at: School of Life and Pharmaceutical Sciences, Dalian University of Technology, China, No. 2 Dagong Road, Panjin, China (Y. Han), Tel.: +86 427-2631889, Fax: +86 427-2631889, E-mail addresses: yanshuohan@dlut.edu.cn (Y. Han)

Department of Orthopedic Surgery, The Third People's Hospital of Shenzhen, Shenzhen 518000, China. Tel.: +86 755-61238928, Fax: +86 755-61238928, E-mail addresses: liujinzhu2005@163.com (J. Liu)

Acknowledgments: None

Word-character count of the complete text: 3478

Abstract

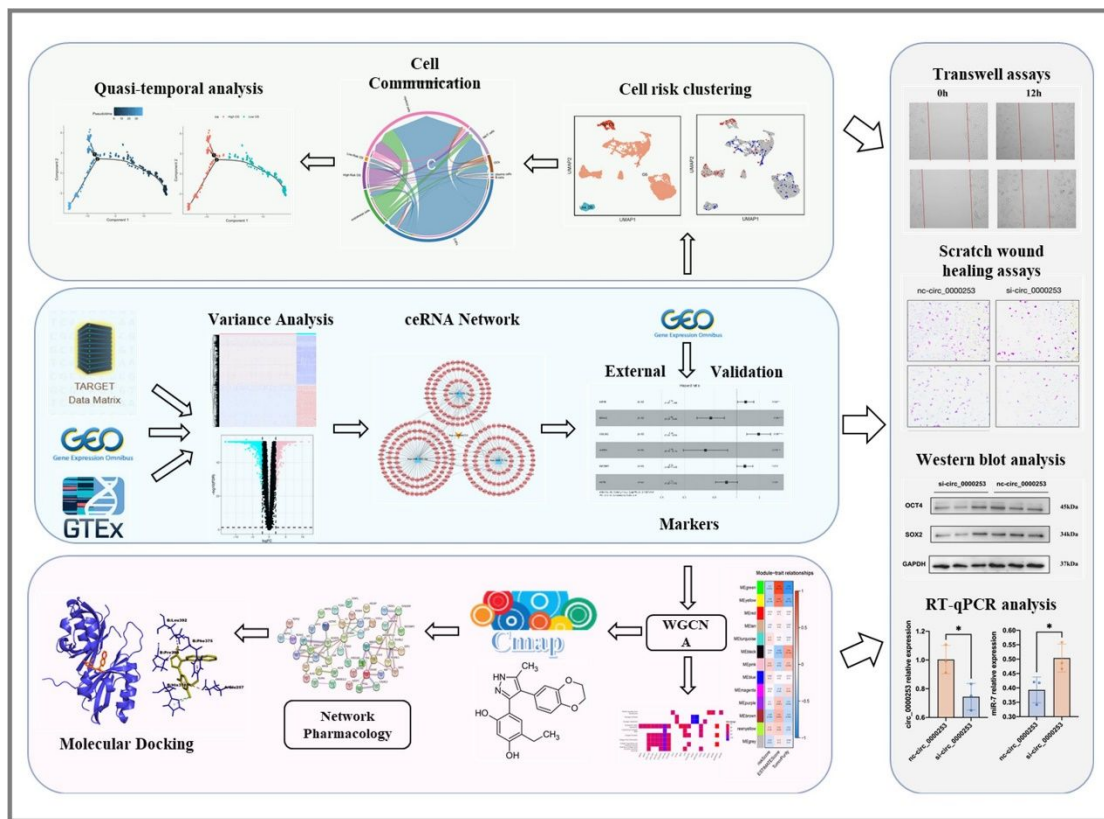
Background: Osteosarcoma (OS) is the most common malignant bone tumor in children and adolescents, characterized by high local infiltration and early metastasis. This study explores the genetic and epigenetic mechanisms underlying OS progression, focusing on the hsa_circ_0000253/miR-7/COL5A2 regulatory axis and the therapeutic potential of CCT-018159.

Methods: Differential expression analysis identified key circRNAs, miRNAs, and mRNAs associated with OS. A ceRNA network centered on hsa_circ_0000253 was constructed, and a Cox risk model was developed using transcriptome data. The impact of the hsa_circ_0000253/miR-7/COL5A2 axis on OS cell proliferation and migration was validated through *in vitro* experiments. Single-cell transcriptome analysis was employed to distinguish high-risk and low-risk OS cell subclusters. Finally, candidate drugs were identified with molecular docking used to assess drug-target interactions.

Results: The study identified nine differentially expressed circRNAs, with hsa_circ_0000253 selected for further investigation due to its significant role in OS progression. The hsa_circ_0000253/miR-7/COL5A2 regulatory axis was shown to be critically involved in OS cell proliferation and migration. *In vitro* experiments demonstrated that knocking down hsa_circ_0000253 and COL5A2 significantly inhibited OS cell proliferation and migration, while knocking down miR-7 had the opposite effect, promoting these processes. Additionally, single-cell transcriptome analysis revealed distinct OS cell subclusters, with high-risk cells showing increased expression of COL5A2, IGF1R, COL1A1, and COL1A2, which were associated with the progression from low-risk to high-risk states. Furthermore, the study identified CCT-018159 as a potential therapeutic agent, significantly inhibiting OS cell proliferation and migration by molecular docking.

Conclusions: The hsa_circ_0000253/miR-7/COL5A2 regulatory axis plays a critical role in OS progression, and CCT-018159 shows promise as a therapeutic agent. Further research is needed to validate these findings *in vivo* and explore the clinical potential of targeting this regulatory axis in OS treatment.

Keywords: Osteosarcoma, circRNA, ceRNA, Cancer Prognosis, Targeted Therapy, Single-cell Transcriptome



Graphical Abstract

This study identifies the *hsa_circ_0000253/miR-7/COL5A2* regulatory axis as a key factor in osteosarcoma progression and highlights CCT-018159 as a promising therapeutic agent, inhibiting cell proliferation and migration.

1. Introduction

Osteosarcoma (OS) is the most common malignant bone tumor, typically occurring in children, adolescents, and young adults¹. OS tends to exhibit high local infiltration and early metastasis, with 30%-50% of individuals observed to have recurrent disease². Approximately 68% of localized OS patients survive 5 years or longer³, but unfortunately, 20%-30% are metastatic or recurrent cases⁴. Despite several anti-cancer substances being used clinically, the prognosis for metastatic and recurrent OS has remained stagnant over the past few decades⁵. These obstacles highlight a desperate need for new treatment strategies to improve the overall survival rates of OS patients.

Circular RNA (circRNA) originates from gene introns or exons and is one of the unique types of non-coding RNAs (ncRNA). Due to its circular structure, compared to linear RNA, circRNA has a more stable structure and is resistant to digestion by exonuclease or RNase R. Competing endogenous RNA (ceRNA) hypothesis points out some ncRNAs, like circRNA, also contain miRNA reactant elements and thus can compete with mRNA to bind with miRNA, indirectly regulating mRNA expression and forming complex post-transcriptional regulation

networks⁶. More and more research show that circRNA also plays crucial roles in osteosarcoma and can promote the development of osteosarcoma through the circRNA-miRNA-mRNA regulatory axis. For instance, CircRNA_0078767 exacerbates osteosarcoma deterioration by increasing CDK3 expression through sponging miRNA-14-330p, and circOMA1 promotes osteosarcoma development by regulating the expression of c-Myc via miR-1294. Also, has_circ_0003732 promotes the progression of osteosarcoma by regulating the miR-377-3p/CPEB1 axis and the Wnt/Beta-catenin signaling pathway⁷⁻⁹. Silencing respective circRNA can inhibit the development of osteosarcoma¹⁰. Single-cell RNA sequencing (scRNA-seq) research of human tumors provides novel insights into tumor heterogeneity and differing subgroups. The research by Yun Liu and others revealed the tumor microenvironment (TME) of osteosarcoma through single-cell transcriptomics and shared the single-cell sequencing data of six OS patients¹¹. Furthermore, current treatments for OS, such as surgical methods, chemotherapy drugs, and immunotherapy drugs, are still ineffective¹². With further research, targeted treatment is becoming irreplaceable.

In this research, we constructed the ceRNA regulatory network and identified the hsa_circ_0000253/miR-7/COL5A2 regulatory axis, the impact of which on OS cell proliferation and invasion was confirmed. Based on the node RNAs of the regulatory network, we built a Cox risk model and validated it using another OS transcriptome cohort. The model hallmark genes IGF1R and COL5A2 overexpression were confirmed by qPCR and western blot experiments. Further, single-cell transcriptomics revealed the differences in collagen signaling pathways of high-risk and low-risk OS cells, and that the expression of COL5A2, IGF1R, COL1A1, and COL1A2 increases with the worsening of OS cells. Lastly, network pharmacology and the Connectivity Map¹³ were employed to screen potential targeted drugs, and CCT-018159 was shown to be able to inhibit the development of OS.

2. Methods

Due to the extensive nature of our methodology, the detailed experimental procedures have been provided in the [Supplementary File - Methods](#). This supplementary material includes comprehensive information on the techniques used for transcriptome analysis, construction of the ceRNA network, in vitro experiments, single-cell transcriptome analysis, and pharmacological screening.

3. Results

3.1 Transcriptome analysis and ceRNA network construction

Differential expression analysis was performed by comparing the expression of circRNA in osteosarcoma samples and control samples within the GEO cohort. Using a threshold of $|logFC| > 2$, nine differentially expressed circRNAs were identified, including three up-regulated

1
2
3 circRNAs (hsa_circ_0010220, hsa_circ_0000253, hsa_circ_0020378) and six down-regulated
4 circRNAs (hsa_circ_0000006, hsa_circ_0046264, hsa_circ_0078767, hsa_circ_0094088,
5 hsa_circ_0096041, has_circ_0049271). [Supplementary File - Table 2](#) for details. Subsequently,
6 with a threshold of false discovery rate (FDR)<0.05 and |logFC|>2, miRNA and mRNA
7 expression data were analyzed by "limma" package ¹⁴, resulting in the identification of 164
8 differentially expressed miRNAs (80 up-regulated and 84 down-regulated) and 2602
9 differentially expressed genes (1190 up-regulated and 1412 down-regulated) ([Figure 1 A-E](#)).
10
11
12
13
14

15 Since the regulatory axes of the up-regulated circRNAs hsa_circ_0010220 and
16 hsa_circ_0020378 have already been reported ^{15,16}, we chose hsa_circ_0000253 as the subject
17 of our study. Next, based on the obtained circRNA-miRNA and miRNA-mRNA relationships,
18 we constructed a circ-mi-m ceRNA network diagram centered on hsa_circ_0000253, which
19 included 3 miRNAs (miR-139-5p, miR-7-5p, and miR-221-3p) and 553 mRNAs ([Supplementary](#)
20 [File - Figure 1](#)). From among these circRNAs, has_circ_253 and miR-7-5p were included in
21 subsequent research. The mRNAs connected to miR-7-5p in the network diagram ([Figure 1 F](#))
22 were used to construct the PPI network diagram ([Figure 1 G](#)). Genes within the PPI network
23 diagram were used for enrichment analysis. The results showed that these genes were
24 enriched significantly in focal adhesion and associated metabolic pathways, and participated in
25 the down-regulation of the apoptosis process ([Figure 1 H-I](#)).
26
27
28
29
30
31
32
33
34
35
36
37
38
39
40
41
42
43
44
45
46
47
48
49
50
51
52
53
54
55
56
57
58
59
60

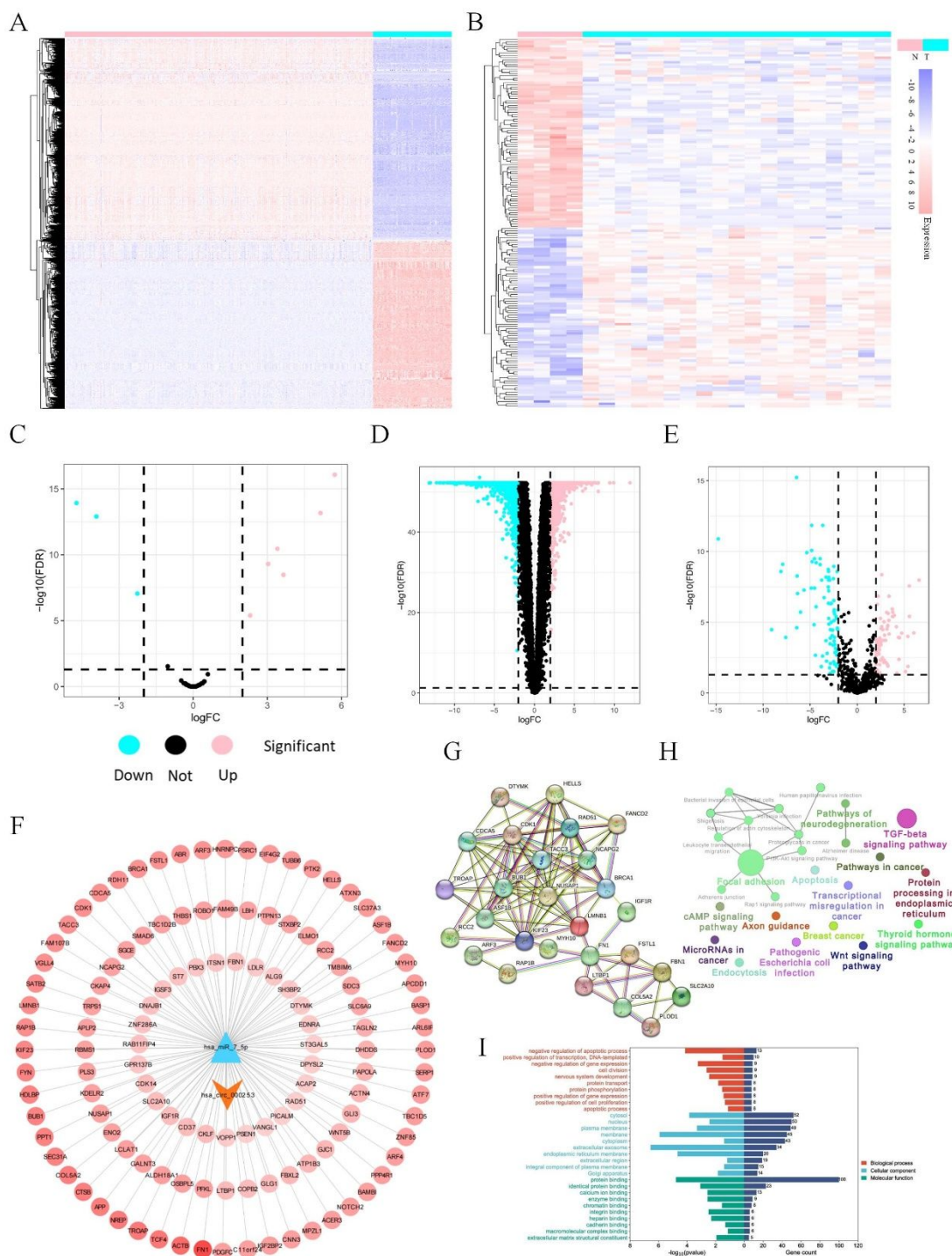


Figure 1. (A-B) Differential analysis heatmaps of mRNA, miRNA and circRNA. (C-E) Differential analysis volcanic maps of mRNA, miRNA and circRNA. (F) CeRNA network with hsa_circ_0000253/miR-7-5p axis. (G) PPI network built by nodes of ceRNA network in Figure 5 F (H-I) GO and Kegg enrichment analysis of genes in the PPI network.

1
2
3 **3.2 Establishment and verification of Cox risk model**
4

5 In the multifactorial Cox analysis, 117 genes were selected from the ceRNA network into the
6 initial model. Lasso regression analysis showed that the lowest cross-validation point of 10
7 genes had significant statistical significance ([Figure 2 A-B](#)). The key genes were further
8 screened using Akaike Information Criterion (AIC) values, and a 6-gene Cox proportional
9 hazard regression model was built, the parameters of the model can be seen in [Table 1](#) and
10 [Figure 2 C-D](#). Subsequently, a nomogram was created to predict the survival probability of OS
11 patients at 1, 3 and 5 years. The area under ROC curve (AUC) of the model for 1, 3, 5 years
12 survival rates were 0.737, 0.841, 0.88, respectively ([Figure 2 E-F](#)), reflecting the discrimination
13 and accuracy of the nomogram along with the correction curve ([Figure 2 G-H](#)). External data
14 validation results from GEO showed that the AUC for 1, 3, 5 years were 0.817, 0.915, 0.921
15 which implied a high accuracy ([Figure 2 I-J](#)). Survival curve analysis showed that in the results
16 of internal and external validation, the survival probability of the high-risk group was significantly
17 lower than that of the low-risk group with respective P-values less than 0.001 and 0.05, and the
18 DCA curve showed that the model has a higher net benefit rate within 1, 3, 5 years of survival.
19
20 ([Figure 2 K-L](#))
21
22
23
24
25
26
27
28
29
30
31
32
33
34
35
36
37
38
39
40
41
42
43
44
45
46
47
48
49
50
51
52
53
54
55
56
57
58
59
60

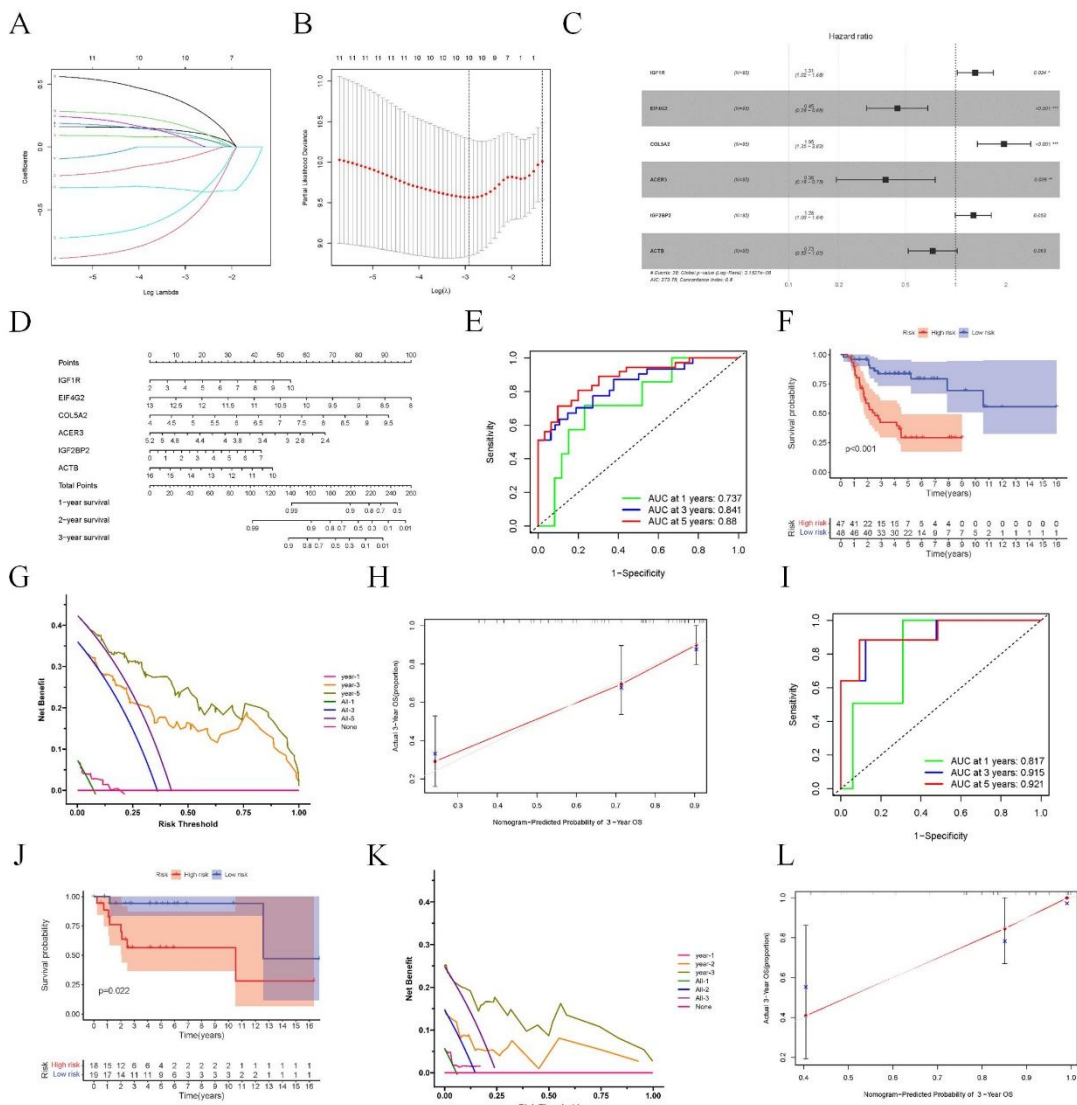


Figure 2. Construction of cox risk prognosis model. (A-B) The results of lasso regression analysis. (C) Forest plot shows prognostic mRNAs signatures of OS. Six potential prognosis related RNAs were integrated into the model. (D) The nomogram was drawn based on the model. (E-H) Internal validation of Cox risk model. E, The ROC curves of 1, 3, and 5-year survivals; F, Survival curves of patients with high/low-risk score based on the model ($p<0.001$); G, The DCA curves of 1, 3, and 5-year survivals. H, Calibration curve of 3-year survival. (I-L) External validation of Cox risk model. I, The ROC curves of 1, 3, and 5-year survivals; J, Survival curves of patients with high/low-risk score based on the model ($p<0.022$); K, The DCA curves of 1, 3, and 5-year survivals. L, Calibration curve of 3-year survival.

Table 1. Parameters of Cox risk model.

| Id | Coef | HR | HR.95L | HR.95H | P-value |
|---------|----------|----------|----------|----------|----------|
| IGF1R | 0.271194 | 1.311529 | 1.021068 | 1.684619 | 0.033738 |
| EIF4G2 | -0.80447 | 0.447324 | 0.293398 | 0.682006 | 0.000185 |
| COL5A2 | 0.668532 | 1.951371 | 1.350722 | 2.819123 | 0.000369 |
| ACER3 | -0.9645 | 0.381175 | 0.192744 | 0.753821 | 0.005567 |
| IGF2BP2 | 0.245271 | 1.277968 | 0.997342 | 1.637554 | 0.052511 |
| ACTB | -0.31546 | 0.729452 | 0.519385 | 1.024482 | 0.0687 |

3.3 hsa_hsa_circ_0000253/miR7/COL5A2 regulating axis is involved in the proliferation and migration of osteosarcoma

In order to further explore the biological function of hsa_circ_0000253/miR7/COL5A2 in osteosarcoma cells, we performed a series of in vitro experiments. We detected cell vitality through MTT experiments, as shown in [Figure 3A](#). After knocking down miR-7 in osteosarcoma cells, the cell proliferation ability was significantly higher than that of the NC group ($P<0.05$). This suggests that the proliferation ability of osteosarcoma cells was significantly increased after knocking down miR-7. After separately knocking down hsa_circ_0000253 and COL5A2, the proliferation ability of osteosarcoma cells was significantly lower than that of the NC group ($P<0.01$). This suggests that the proliferation ability of osteosarcoma cells was significantly inhibited after knocking down hsa_circ_0000253 and COL5A2. We detected cell migration through scratch experiments and Transwell experiments. We respectively knocked down hsa_circ_0000253 and COL5A2, and took photos for inspection at 12h, 24h, and 48h. As shown in [Figure 3 C-E](#), the remaining area of cell healing was significantly lower than the NC group ($P<0.05$). At the same time, in [Figure 3B](#), Transwell experiments also proved that after inhibiting the expression of hsa_circ_0000253, the number of osteosarcoma cells that migrated to the lower chamber significantly decreased ($P<0.01$). The above research proves that the migration ability of osteosarcoma cells is significantly inhibited after knocking down hsa_circ_0000253 and COL5A2. However, after knocking down miR-7, the remaining area of cell healing in osteosarcoma cells is significantly higher than the NC group ($P<0.05$), suggesting that knocking down miR-7 significantly promotes the migration ability of osteosarcoma cells. qRT-PCR results show that the knockdown effect of hsa_circ_0000253 is significant, knocking down hsa_circ_0000253 promotes the expression of miR-7 and inhibits the expression of COL5A2; the knockdown effect of COL5A2 is significant, knocking down COL5A2 significantly inhibits the proliferation of osteosarcoma cells ($P<0.05$). The above results initially verify the regulation axis of hsa_circ_0000253/miR7/COL5A2 ([Figure 3 F-J](#)). We detected the expression of tumor stemness genes SOX2 and OCT4 after knocking down hsa_circ_0000253 by Western blot experiment ([Figure 3K](#)). The results show that inhibiting the expression of hsa_circ_0000253 will inhibit the expression of tumor stemness genes SOX2 and OCT4, further highlighting the carcinogenic role (collagen protein V, E-cadherin and β -catenin) of hsa_circ_0000253 (also in

Figure 3K). At the same time, we also detected the expression of collagen protein V, E-cadherin and β -catenin in cells after knocking down COL5A2 (Figure 3 L). The results revealed that after knocking down hsa_circ_0000253 and COL5A2, the expression of collagen protein V in osteosarcoma cells was reduced, the expression of E-cadherin was increased and the expression of β -catenin had no significant change. This suggested that after knocking down hsa_circ_0000253, the expression of COL5A2 was inhibited and hsa_circ_0000253 and COL5A2 could affect the EMT of osteosarcoma cells. Knocking down hsa_circ_0000253 and COL5A2 may improve osteosarcoma disease.

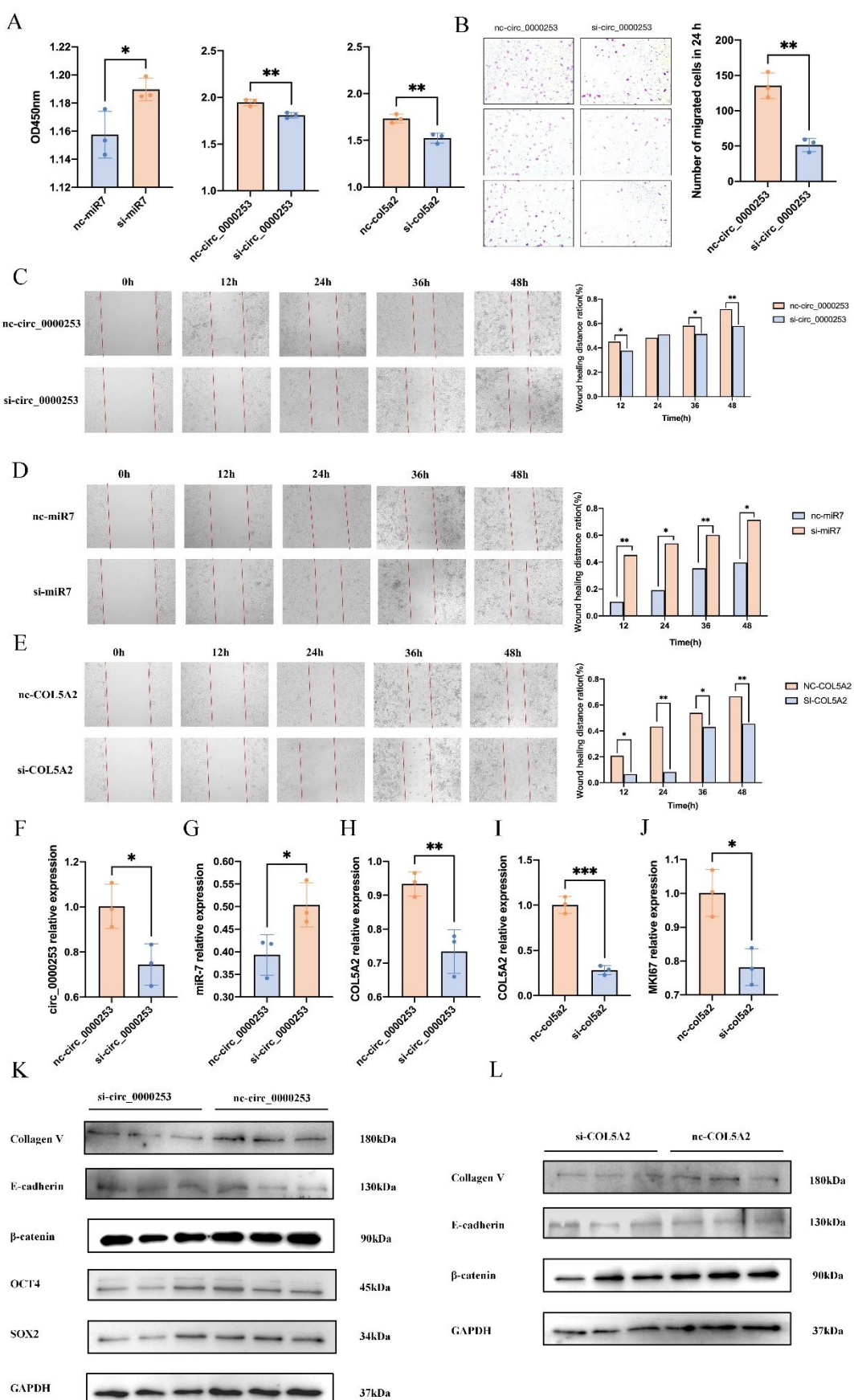
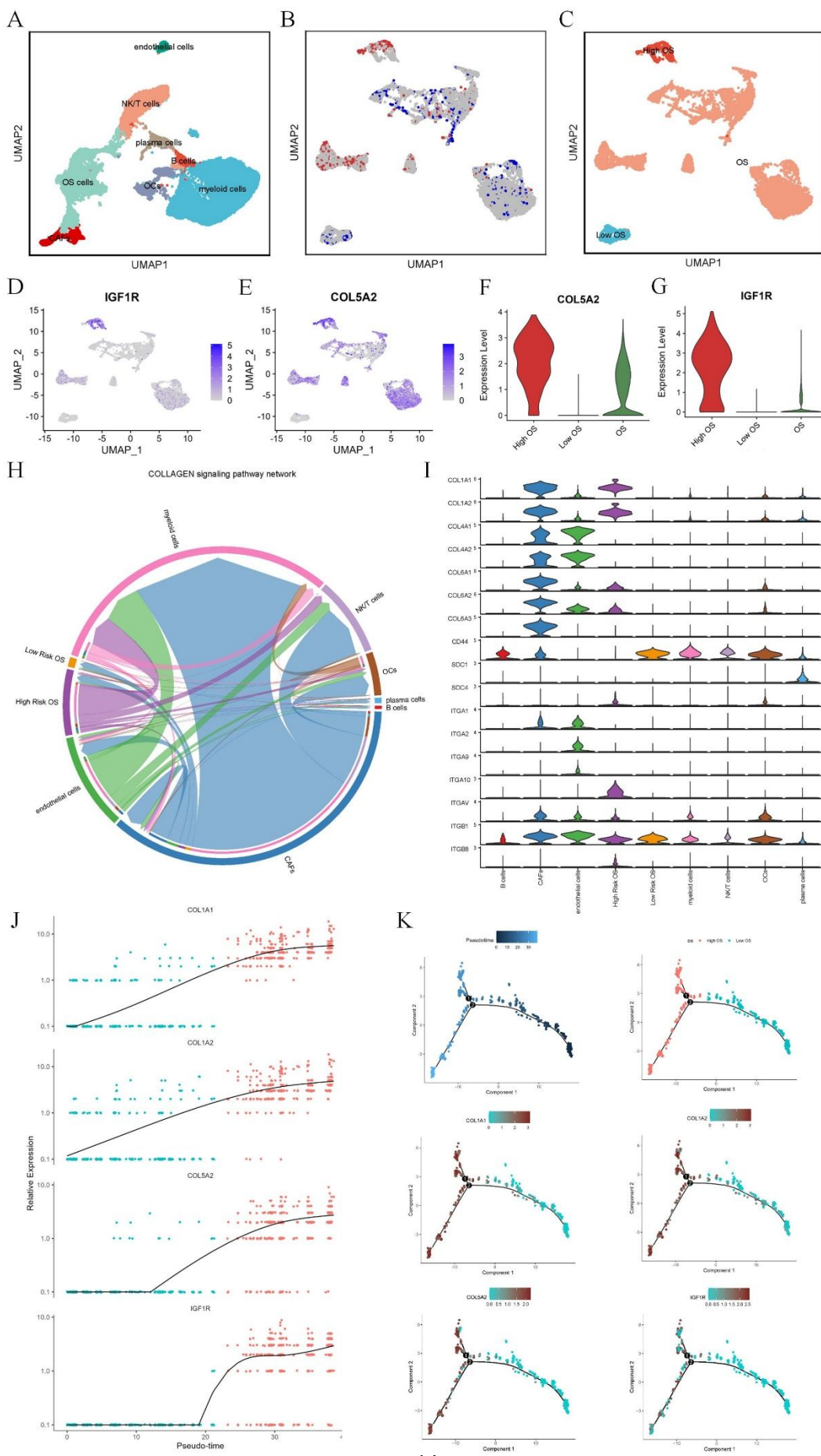


Figure 3. (A) MTT detected the effects of transfection of miR-7, circ_0000253 and COL5A2 on

the proliferation of osteosarcoma cells. (B) Transwell assay was used to detect the effects of circ_0000253 transfection on the migration of osteosarcoma cells, images were taken 24h after transfection. (C-E) The effects of transfection with circ_0000253, miR-7 and COL5A2 on the migration of osteosarcoma cells was respectively detected by scratch assay, the cell migration was recorded at 0 h, 12 h, 24 h, 36 h and 48 h, respectively. (F-J) qRT-PCR preliminatively verified the knockdown effects of circ_0000253/miR-7/COL5A2 axis; F, the circ_0000253 knockdown effect is remarkable; G, Knockdown circ_0000253 promoted the expression of miR-7; H, Knockdown circ_0000253 inhibited the expression of COL5A2; I, the knock down effect of COL5A2 is remarkable; J, COL5A2 knockdown significantly inhibited the proliferation of osteosarcoma cells. (K) The expression of tumor stem genes, OCT4 and SOX2, and collagen V, E-cadherin and β -catenin after knocking down circ_0000253. (L) The expression of collagen V and EMT markers, E-cadherin and β -catenin, in osteosarcoma cells after knockdown COL5A2. *P<0.05, **P<0.01, ***P<0.001.

3.4 Single cell transcriptome reveals osteosarcoma development

The results of cell clustering and annotation in the OS single cell transcriptome are shown in [Figure 4 A](#). From these, we extracted the OS cell clusters and re-clustered them to obtain 7 distinct OS sub-cell clusters ([Supplementary File - Figure 2](#)). Next, as shown in [Figure 4 B](#), we used the R package Scissor to annotate the OS cells as high-risk¹⁷ and low-risk (blue). Combining Scissor's cell typing and the expression distribution of the marker genes COL5A2 and IGF1R ([Figure 4 D-E](#)), which had been validated in the cox risk model, we identified the high-risk OS cell sub-clusters (hOSC) and low-risk OS cell sub-clusters (IOSC) ([Figure 4 C](#)). As shown in Figures 4 F-G, the expression of COL5A2 and IGF1R in hOSC is much higher than in IOSC. Figure 4H shows the analysis results of the collagen signaling pathway. In this pathway, hOSC sends clear communication signals to other types of cells such as myeloid cells and NK/T cells, while IOSC is the opposite. There are no significant differences in signal reception between the two types of OS cells. Further, Figure 4I shows that the expression of genes involved in the collagen signaling pathway is significantly higher in hOSC than in IOSC, such as COL1A1 and COL1A2. We extracted hOSC and IOSC cells for pseudo-time analysis and found that IOSC gradually develops into hOSC over time. In this process, changes in the expression of COL1A1, COL1A2, COL5A2, and IGF1R are shown in [Figure 4J](#). The expression levels of these four genes continuously increased over time with COL1A1 and COL1A2 showing a clear correlation with the development of OS from low-risk to high-risk ([Figure 4K](#)). In the single cell transcriptome, the gene set was sorted from high to low according to the LogFC value of hOSC relative to IOSC and was used for GSEA in the GO database. Based on GSEA, multiple collagen-related GOs had been found to be significantly overexpressed in hOSC ([Supplementary File - Figure 3A](#)). In addition, [Supplementary File - Figure 3B](#) shows that compared to the controls, collagen-related GOs are significantly enriched in AAAs.



1
2
3 **Figure 4.** (A) Umap plot of 8 kinds of cells from 6 OS patients. (B) Scissors divided OS cells
4 into high risk and low risk. Red: high risk OS cells, Blue: low risk OS cells. (C) Umap plot of OS
5 cell clusters. Red: hOSC, Blue: IOSC. (D-E) Umap plots of expression of IGF1R and COL5A2.
6 (F-G) Violin plots show expression of IGF1R and COL5A2 in different OS cell clusters. (H)
7 Chord diagram reveals the cell communication among hOSC, IOSC and seven other kinds of
8 cell. (I) Violin plots of genes in Collagen signal pathway. (J) Six trajectory plots show
9 Pseudotime, high and low clusters, and expression of COL1A1, COL1A2, COL5A2 and IGF1R
10 in the process of OS cell development. (K) The increase of expression of COL1A1, COL1A2,
11 COL5A2 and IGF1R with Pseudotime are indicated in four scatter diagrams.
12
13
14
15
16
17
18
19

20 *3.5 CCT-018159 is a candidate drug to inhibit the development of osteosarcoma*
21

22 Through ssGSEA, the expression patterns of 29 immune indicators in the high-risk and low-risk
23 groups were analyzed, as seen in [Figure 5A](#). [Figure 5 B-C](#) shows that the ESTIMATE score of
24 the low-risk group is significantly higher than the high-risk group, while tumor purity is the
25 opposite. Based on WGCNA, we obtained the correlation between the differential gene clusters
26 and risk score, ESTIMETES score, and tumor purity ([Figure 5D](#)). Among them, the yellow
27 module has the highest negative correlation value with the risk score (-0.36), and it also has a
28 high correlation with the immune score and tumor purity (0.63 and -0.59), while the pink module
29 has the highest positive correlation with the risk score (0.24) and a significant correlation with
30 the other two features (-0.25 and 0.27). The upregulated genes in the yellow module are largely
31 enriched in Neutrophil degranulation and MHC class II antigen presentation ([Supplementary](#)
32 [File - Figure 4A](#)). In the enrichment results of the pink module, the role of the COL family is
33 particularly prominent. These differentially expressed COL family genes include COL11A2,
34 COL13A1, COL22A1, COL24A1, COL4A4 and COL5A2, all of which play a key role in the
35 collagen-related pathway ([Supplementary File - Figures 4B](#)). After inputting the genes from the
36 yellow and pink modules into CMap analysis, the top 50 results of drugs acting on the U2OS
37 cell line were screened out and intersected ([Supplementary File - Table 3](#) and [Supplementary](#)
38 [File - Table 4](#)), obtaining 5 potential anti-OS drugs ([Figure 5E](#)). The targets of the top-ranked
39 candidate drug CCT-018159 were predicted by PharmMapper and SuperPred with thresholds
40 of Norm Fit>0.5 and Probability>0.5 respectively, resulting in 322 shared drug target genes.
41 DisGeNET and OMIM platforms could both retrieve 847 OS targets. The intersection of two
42 gene sets (322 drug targets and 847 OS targets) resulted in 30 genes whose PPI networks are
43 shown in [Figure 5 G](#), expression differences are shown in [Figure 5H](#) and functional enrichment
44 results are shown in the [Supplementary File - Figure 5 A-D](#).
45
46
47
48
49
50
51
52
53
54

55
56 The enrichment score of the target genes in the HIF-1 signaling pathway is high and the over-
57 expressed gene HIF1A is a hub in the PPI network. Therefore, next, we used AutoDock Vina
58 to dock HIF1A as a receptor with CCT-018159 and used Discover Studio (version 4.5.0) to
59
60

analyze the interaction force. Results are shown in Figure 5I and Supplementary File - Figure 6 A-B. The molecular affinity of the optimal conformation is -6.4 kcal/mol. After treating MG-63 cells with different concentrations of CCT-018159 (0 μ M, 10 μ M, 20 μ M, 30 μ M, 40 μ M, 50 μ M), the CCK-8 results showed that the drug at 30 μ M significantly inhibited the proliferation of MG-63 cells. Furthermore, when cells were treated with 40 μ M or 50 μ M concentrations of the drug, cell proliferation was almost completely suppressed, even inducing cell death (Figure 5J). The scratch assay results also indicated that after treating MG-63 cells with 40 μ M CCT-018159 for 24 hours, cell migration was significantly inhibited, suggesting that CCT-018159 may play an important role in the treatment of osteosarcoma (Figure 5K).

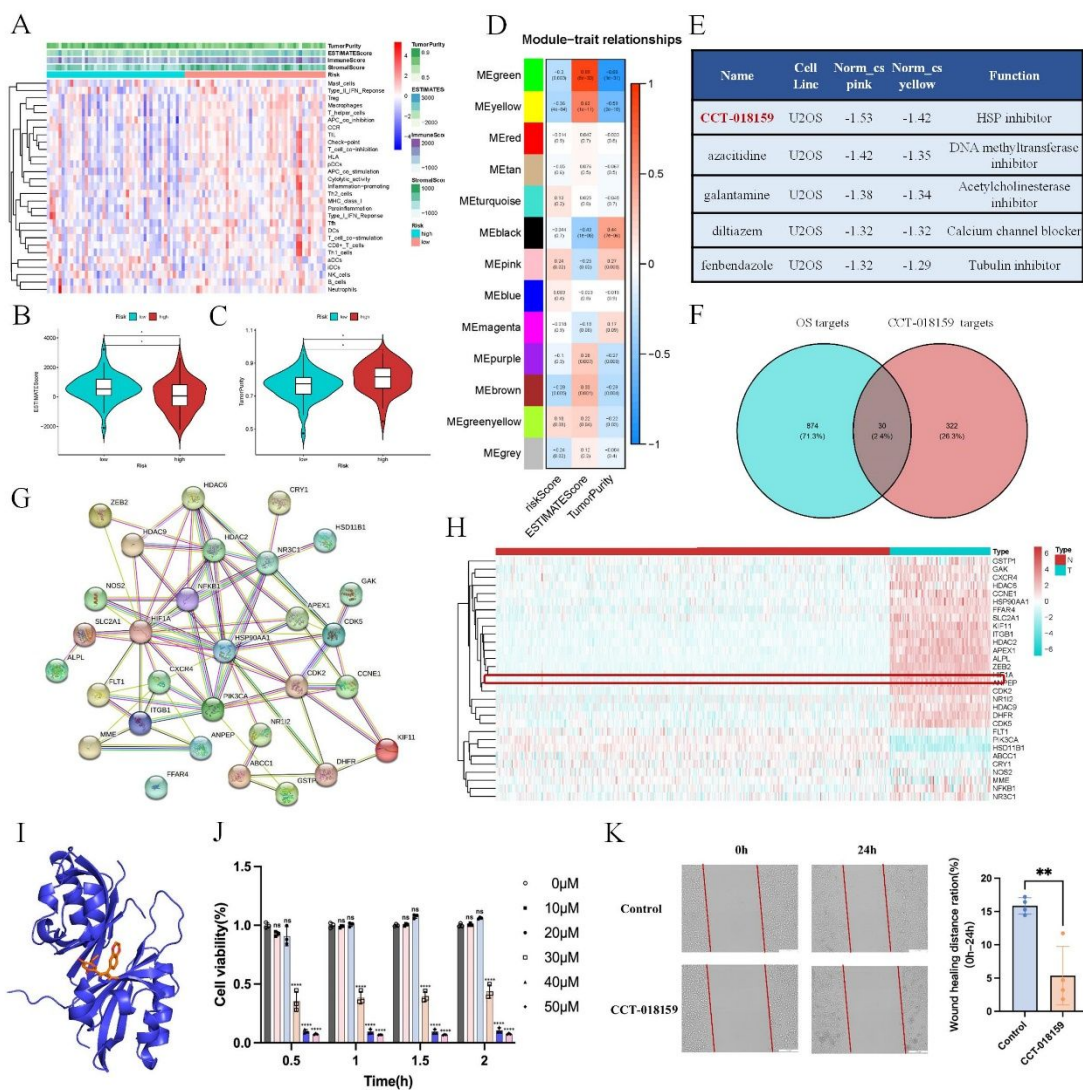


Figure 5. The heatmap (A) shows the ssGSEA results of 26 immune markers between high- and low- risk groups. The upper part of the heatmap shows tumor purity, ESTIMATE score immune score and stromal score in OS patients. Two violin charts (B-C) show the differences in ESTIMATE score and tumor purity between high-risk and low-risk OS patients. The results of wilcox test reveal that ESTIMATE score of low-risk group are all significantly lower than high-risk group, while tumor purity is just the opposite which is higher in high-risk group. (D) WGCNA

of DEGs on risk score, ESTIMATE score and tumor purity. (E) Names, cell lines, norm connectivity scores in both pink and yellow gene clusters and functions of five candidate drugs. The lower the norm connectivity scores, the better the inhibitory effect on osteosarcoma. Venn diagram (F) shows the intersection of targets. (G) PPI network of the target proteins. Heatmap (H) shows the expression of target genes between control and OS samples. (I) Results of molecular docking and interaction analysis between CCT-018159 and protein 4H6J. (J) CCK-8 detected the proliferation of osteosarcoma cells when the concentration of CCT-018159 was 0µM, 10µM, 20µM, 30µM, 40µM, 50µM, respectively (K) The migration of osteosarcoma cells at 40µM concentration of CCT-018159 was detected by wound healing test. (*P<0.05, **P<0.01, ***P<0.001, ****P<0.0001)

4. Discussion

Circular RNAs play a vital role in regulating tumor progression. Hsa_circ_0000253 plays a significant part in the development of osteosarcoma, but very few studies explore its exact working mechanism. From our analysis of osteosarcoma transcriptome data, we built a circ-miRNA-mRNA network centered on hsa_circ_0000253. The miRNAs include miR-139-5p, miR-7-5p, and miR-221-3p. Current research indicates that miR-139-5p, miR-7-5p, and miR-221-3p all affect the development of osteosarcoma to varying degrees¹⁸⁻²³, with most research focused on miR-7-5p. However, there has been no reported research on how hsa_circ_0000253 influences miR-7-5p, affecting the development of osteosarcoma.

COL5A2 has been shown to play a significant role in various cancers like rectal, gastric and ovarian cancers²⁴⁻²⁶. Studies have shown that COL5A2 inhibits the TGF-β and Wnt/β-Catenin signaling pathways, preventing the invasion and metastasis of osteosarcoma²⁷. Our bioinformatics predictions show a high likelihood of interaction between COL5A2 and miR-7-5p. In the meanwhile, we have found that down-regulating miR-7-5p enhances osteosarcoma cell proliferation and migration, whereas down-regulation of hsa_circ_0000253 and COL5A2 inhibits them. Both hsa_circ_0000253 and COL5A2 were found to affect collagen-related protein expression inside osteosarcoma cells, suggesting their involvement in osteosarcoma cells' epithelial-mesenchymal transition (EMT). By analyzing single-cell data, we identified seven different subgroups of osteosarcoma cells. Based on the expression levels of COL5A2 and IGF1R, we categorized the osteosarcoma cells into high-risk (hOSC) and low-risk (IOSC) subgroups. Analysis of the collagen signaling pathway showed that the genes involved in this pathway were significantly upregulated in hOSC and exhibited active communication with other cell types. Moreover, the expression of COL1A1, COL1A2, COL5A2, and IGF1R increased over time, indicating their connection with the progression of osteosarcoma from low to high risk.

CCT-018159 is known to induce cell apoptosis and inhibit key endothelial and tumor cell

functions related to invasion and angiogenesis²⁸, but its role in osteosarcoma treatment is unclear. To find potential treatment options, we analyzed the expression patterns of immune-related genes and identified candidate drugs using ssGSEA, ESTIMATE, and WGCNA. Combining the Cmap analysis results with the target prediction results, we identified CCT-018159 as a potential drug for osteosarcoma treatment. Additionally, we demonstrated experimentally that CCT-018159 significantly inhibits osteosarcoma cell proliferation and migration, suggesting it may be a potential therapeutic drug for osteosarcoma. However, the specific action mechanism of CCT-018159 in human treatments is unclear and requires further research to explore its role in treating osteosarcoma.

In this study, we conducted a comprehensive analysis of the transcriptome and ceRNA network in osteosarcoma (OS). We identified differentially expressed circRNAs, miRNAs, and mRNAs in OS samples compared to control samples. Based on the ceRNA network, we constructed a circ-miRNA-mRNA network centered around hsa_circ_0000253, which included miR-139-5p, miR-7-5p, and miR-221-3p. We further investigated the biological functions of the hsa_circ_0000253/miR7/COL5A2 regulatory axis in OS through in vitro experiments. The results showed that downregulation of miR-7 enhanced cell proliferation, while downregulation of hsa_circ_0000253 and COL5A2 inhibited cell proliferation. Additionally, cell migration was suppressed by downregulating hsa_circ_0000253 and COL5A2, while it was promoted by downregulating miR-7. The expression of tumor stemness genes SOX2 and OCT4 was also inhibited by downregulating hsa_circ_0000253. Furthermore, the expression of collagen-related proteins was altered, indicating the involvement of hsa_circ_0000253 and COL5A2 in the EMT of OS cells.

To gain insights into the development of OS at the single-cell level, we performed single-cell transcriptome analysis and identified seven distinct subclusters of OS cells. Using the Scissor package, we classified OS cells into high-risk (hOSC) and low-risk (lOSC) subclusters based on their expression patterns and the validated marker genes COL5A2 and IGF1R. The hOSC subcluster exhibited higher expression levels of COL5A2 and IGF1R compared to the lOSC subcluster. Analysis of collagen signaling pathways revealed that genes involved in this pathway were significantly upregulated in hOSC, and hOSC showed active communication with other cell types. Moreover, the expression of COL1A1, COL1A2, COL5A2, and IGF1R increased over time, indicating their association with the progression from low-risk to high-risk OS.

In the search for potential therapeutic options, we analyzed the expression patterns of immune-related genes and identified candidate drugs using ssGSEA, ESTIMATE, and WGCNA. The yellow module was negatively correlated with the risk score and positively correlated with immune score and tumor purity. The pink module showed the opposite correlation pattern. The enrichment analysis highlighted the role of the COL family genes, including COL5A2, in

1
2
3 collagen-related pathways. By intersecting the results of Cmap analysis and target prediction,
4 we identified CCT-018159 as a potential drug for OS treatment. The molecular docking analysis
5 indicated a strong interaction between CCT-018159 and the HIF1A receptor. Additionally, we
6 demonstrated through experiments that CCT-018159 significantly inhibited the proliferation and
7 migration of osteosarcoma cells, suggesting that it may be used as a therapeutic drug for
8 osteosarcoma. However, the toxic effects of CCT-018159 are still not clear, and further
9 research is needed to explore its potential use in osteosarcoma treatment.
10
11

12
13 In this study, we have uncovered the influential role of the hsa_circ_0000253/miR-7/COL5A2
14 regulatory axis in the progression of osteosarcoma and identified CCT-018159 as a potential
15 therapeutic agent. Our work aligns with the scientific objectives of Molecular Therapy - Nucleic
16 Acids, focusing on gene- and oligonucleotide-based therapies for genetic and acquired
17 diseases. Strengths: Our study provides a comprehensive investigation into the molecular
18 mechanisms at play in osteosarcoma, combining bioinformatics analyses with *in vitro*
19 experiments for a multifaceted approach. This rigorous methodology enables us to uncover the
20 significance of the hsa_circ_0000253/miR-7/COL5A2 axis in the disease's pathogenesis.
21 Moreover, the identification of CCT-018159 as a potential therapeutic agent offers a promising
22 new direction for osteosarcoma treatment. Our findings contribute to the ongoing development
23 of nucleic-acid-based therapeutics, showcasing the potential of circRNA-based regulatory axes
24 as effective treatment targets. Limitations: While our study offers valuable insights into
25 osteosarcoma's molecular landscape, several limitations warrant consideration. First, our
26 research lacks *in vivo* validation, which would strengthen the conclusions drawn from our *in*
27 *vitro* experiments. Second, our sample size and diversity are limited. Expanding the population
28 sample would enhance the generalizability of our findings. Lastly, although we have identified
29 CCT-018159 as a potent therapeutic agent, further studies are needed to elucidate its precise
30 mechanism of action and evaluate its safety and efficacy in clinical settings. Despite these
31 limitations, our study holds significant potential to shape osteosarcoma therapy advancements,
32 paving the way for future research to further explore nucleic-acid-based treatment strategies.
33
34

35 Possible mechanisms: The hsa_circ_0000253/miR7/COL5A2 regulatory axis identified in this
36 study may contribute to osteosarcoma development through several possible mechanisms:
37 firstly, regulation of proliferation and migration: Downregulation of hsa_circ_0000253 and
38 COL5A2, as well as upregulation of miR-7, were associated with suppressed cell proliferation
39 and migration in osteosarcoma cells. These molecules may modulate key signaling pathways
40 involved in cell cycle progression, apoptosis, and cell motility. Secondly, EMT, the altered
41 expression of collagen-related proteins, including COL5A2, suggests a potential role in EMT, a
42 process that enables cancer cells to acquire invasive and migratory properties. The
43 hsa_circ_0000253/miR7/COL5A2 axis may influence EMT-related signaling pathways, leading
44 to changes in cell morphology and behavior. Simultaneously, Tumor stemness regulation: The
45 downregulation of hsa_circ_0000253 was associated with the inhibition of tumor stemness
46

genes SOX2 and OCT4. This suggests that hsa_circ_0000253 may play a role in maintaining the stemness properties of osteosarcoma cells, which are associated with tumor initiation, progression, and treatment resistance. Lastly, interaction with the tumor microenvironment: The ceRNA network and single-cell transcriptome analysis revealed communication between osteosarcoma cells and other cell types, such as myeloid cells and NK/T cells. This interaction may affect the tumor microenvironment and contribute to tumor progression and immune evasion.

This study presented compelling evidence for the role of the hsa_circ_0000253/miR7/COL5A2 regulatory axis in OS development and progression. By utilizing an integrative approach, we reaffirmed the importance of this regulatory axis in OS proliferation, migration, and potential involvement in EMT. Additionally, we unveiled potential links between this axis, tumor stemness regulation, and changes in the tumor microenvironment. Importantly, the downregulation of this axis was associated with the inhibition of tumor stemness genes – a promising avenue for future cancer therapeutics. Our comprehensive approach provided meaningful insights into the potential mechanisms of OS and underlying communication between various cell types within the tumor milieu. Furthermore, the identification of the candidate drug CCT-018159, alongside its strong interaction with the HIF1A receptor, underscores the therapeutic implications of these findings. Despite these promising results, the need for *in vivo* validations and more detailed mechanistic investigations remains. Increased sample size and reduced sample diversity are necessary to expand the generalizability of our findings. Future work should additionally focus on the precise mechanisms by which the hsa_circ_0000253/miR7/COL5A2 axis influences cellular processes in OS.

5. Conclusion

In conclusion, our study sheds light on the critical role the hsa_circ_0000253/miR-7/COL5A2 regulatory axis plays in the progression of osteosarcoma. It provides a comprehensive understanding of the underlying molecular mechanisms and identifies CCT-018159 as a potential therapeutic agent. These findings point towards the vast potential of circRNA-based regulatory axes as effective treatment targets for genetic and acquired diseases like osteosarcoma. Our results support the mission of Molecular Therapy - Nucleic Acids of advancing gene- and oligonucleotide-based therapies, and signify a considerable leap in the development of nucleic-acid-based therapeutics. Although future research is warranted to validate our findings *in vivo* and unravel the exact operational mechanisms of CCT-018159, our study contributes to the evolving body of knowledge on osteosarcoma and opens a novel therapeutic avenue for its treatment.

6. Data availability statement

The data that support the findings of this study are available from the corresponding author upon reasonable request.

7. Acknowledgments

None.

8. Author's contributions

Yanshuo Han, Jinzhu Liu, and Xu Guo conceived, designed, performed the study; Xiangrui Zhu, Xin Tian, and Yunfeng Dai carried out the experiments; Xu Guo, Xiangrui Zhu and Mahmoud A.A Ibrahim analyzed the data; Xu Guo, Xiangrui Zhu, Yanshuo Han and Batchimeg Tsedenbal wrote the manuscript; Yanshuo Han, Jinzhu Liu and Mahmoud A.A Ibrahim revised the manuscript. All authors read and approved the final manuscript.

9. Funding sources

This work was supported by the Fundamental Research Funds for the Central Universities (grant number: DUT22YG107), the National Natural Science Foundation of China (grant number: 81600370), the China Postdoctoral Science Foundation (grant number: 2018M640270) and the Natural Science Foundation of Liaoning Province (2023-MS-096).

10. Ethic statement

This research utilized publicly available data and established cell lines, and did not involve any direct interaction with human or animal subjects. As such, no specific ethical approval was required for the studies conducted. All data used in this research were obtained from publicly accessible databases in compliance with their respective usage guidelines.

11. Conflict of Interest

None.

12. References

- Chen C, Xie L, Ren T, Huang Y, Xu J, Guo W. Immunotherapy for osteosarcoma: Fundamental mechanism, rationale, and recent breakthroughs. *Cancer Letters*. 2021/03/01/2021;500:1-10. doi:<https://doi.org/10.1016/j.canlet.2020.12.024>
- Berhe S, Danzer E, Meyers PA, Behr G, LaQuaglia MP, Price AP. Unusual abdominal metastases in osteosarcoma. *Journal of Pediatric Surgery Case Reports*. 2018/01/01/2018;28:13-16. doi:<https://doi.org/10.1016/j.epsc.2017.09.022>
- Chen C-I, Zhang L, Jiao Y-r, et al. miR-134 inhibits osteosarcoma cell invasion and metastasis through targeting MMP1 and MMP3 in vitro and in vivo. <https://doi.org/10.1002/1873-3468.13387>. *FEBS Letters*. 2019/05/01 2019;593(10):1089-1101. doi:<https://doi.org/10.1002/1873-3468.13387>
- Wedekind MF, Wagner LM, Cripe TP. Immunotherapy for osteosarcoma: Where do we go from here? Review. *Pediatric Blood and Cancer*. 2018;65(9)e27227. doi:10.1002/pbc.27227
- Lussier DM, Johnson JL, Hingorani P, Blattman JN. Combination immunotherapy with α -CTLA-4 and α -PD-L1 antibody blockade prevents immune escape and leads to complete

- control of metastatic osteosarcoma. Article. *Journal for ImmunoTherapy of Cancer*. 2015;3(1)21. doi:10.1186/s40425-015-0067-z
6. Salmena L, Poliseno L, Tay Y, Kats L, Pandolfi PP. A ceRNA hypothesis: the Rosetta Stone of a hidden RNA language? *Cell*. Aug 5 2011;146(3):353-8. doi:10.1016/j.cell.2011.07.014
7. Shi Y, Tian Y, Sun X, Qiu Y, Zhao Y. Silencing circOMA1 Inhibits Osteosarcoma Progression by Sponging miR-1294 to Regulate c-Myc Expression. *Frontiers in oncology*. 2022;12:889583. doi:10.3389/fonc.2022.889583
8. Zhang G, Zhu Y, Jin C, et al. CircRNA_0078767 promotes osteosarcoma progression by increasing CDK14 expression through sponging microRNA-330-3p. *Chemico-biological interactions*. Jun 1 2022;360:109903. doi:10.1016/j.cbi.2022.109903
9. Zhou Z, Liu T, Li Z, Wang L. Circ_0003732 promotes osteosarcoma progression through regulating miR-377-3p/CPEB1 axis and Wnt/β-catenin signaling pathway. *Anti-cancer drugs*. Jan 1 2022;33(1):e299-e310. doi:10.1097/cad.0000000000001206
10. Liu J, Yang L, Fu Q, Liu S. Emerging Roles and Potential Biological Value of CircRNA in Osteosarcoma. *Frontiers in oncology*. 2020;10:552236. doi:10.3389/fonc.2020.552236
11. Liu Y, Feng W, Dai Y, et al. Single-Cell Transcriptomics Reveals the Complexity of the Tumor Microenvironment of Treatment-Naive Osteosarcoma. *Frontiers in oncology*. 2021;11:709210. doi:10.3389/fonc.2021.709210
12. Hu Z, Wen S, Huo Z, et al. Current Status and Prospects of Targeted Therapy for Osteosarcoma. *Cells*. Nov 5 2022;11(21)doi:10.3390/cells11213507
13. Lamb J, Crawford ED, Peck D, et al. The Connectivity Map: using gene-expression signatures to connect small molecules, genes, and disease. *Science (New York, NY)*. Sep 29 2006;313(5795):1929-35. doi:10.1126/science.1132939
14. Ritchie ME, Phipson B, Wu D, et al. limma powers differential expression analyses for RNA-sequencing and microarray studies. *Nucleic acids research*. Apr 20 2015;43(7):e47. doi:10.1093/nar/gkv007
15. Deng R, Cui X, Dong Y, et al. Construction of circRNA-Based ceRNA Network to Reveal the Role of circRNAs in the Progression and Prognosis of Hepatocellular Carcinoma. *Frontiers in genetics*. 2021;12:626764. doi:10.3389/fgene.2021.626764
16. Lu Z, Wang C, Lv X, Dai W. Hsa_circ_0010220 regulates miR-198/Syntaxin 6 axis to promote osteosarcoma progression. *Journal of bone oncology*. Jun 2021;28:100360. doi:10.1016/j.jbo.2021.100360
17. The GC, Aguet F, Anand S, et al. The GTEx Consortium atlas of genetic regulatory effects across human tissues. *Science*. 2020/09/11 2020;369(6509):1318-1330. doi:10.1126/science.aaz1776
18. Gu W, Chen P, Ren P, Wang Y, Li X, Gong M. Downregulation of TAF9B by miR-7-5p Inhibits the Progression of Osteosarcoma. *OncoTargets and therapy*. 2021;14:2917-2927. doi:10.2147/ott.S264786
19. Chen H, Chen J. LncRNA SOX21-AS1 Promotes the Growth and Invasiveness of Osteosarcoma Cells Through miR-7-5p/IRS2 Regulatory Network. *Archives of medical research*. Apr 2021;52(3):294-303. doi:10.1016/j.arcmed.2020.11.007
20. Liu W, Long Q, Zhang W, et al. miRNA-221-3p derived from M2-polarized tumor-associated macrophage exosomes aggravates the growth and metastasis of osteosarcoma

- 1 through SOCS3/JAK2/STAT3 axis. *Aging.* Aug 13 2021;13(15):19760-19775.
2 doi:10.18632/aging.203388
- 3 21. Zhang W, Wang Q, Du H, Jiang S. CRISPR/Cas9-mediated overexpression of long non-
4 coding RNA SRY-box transcription factor 21 antisense divergent transcript 1 regulates the
5 proliferation of osteosarcoma by increasing the expression of mechanistic target of rapamycin
6 kinase and Kruppel-like factor 4. *Bioengineered.* Mar 2022;13(3):6678-6687.
7 doi:10.1080/21655979.2021.1995106
- 8 22. Wu J, Zhang T, Chen Y, Ha S. MiR-139-5p influences hepatocellular carcinoma cell
9 invasion and proliferation capacities via decreasing SLTRK4 expression. *Bioscience reports.*
10 May 29 2020;40(5)doi:10.1042/bsr20193295
- 11 23. Zhang S, Chen R. LINC01140 regulates osteosarcoma proliferation and invasion by
12 targeting the miR-139-5p/HOXA9 axis. *Biochemistry and biophysics reports.* Sep
13 2022;31:101301. doi:10.1016/j.bbrep.2022.101301
- 14 24. Wang J, Jiang YH, Yang PY, Liu F. Increased Collagen Type V α 2 (COL5A2) in Colorectal
15 Cancer is Associated with Poor Prognosis and Tumor Progression. *OncoTargets and therapy.*
16 2021;14:2991-3002. doi:10.2147/ott.S288422
- 17 25. Feng S, Xu Y, Dai Z, Yin H, Zhang K, Shen Y. Integrative Analysis From Multicenter
18 Studies Identifies a WGCNA-Derived Cancer-Associated Fibroblast Signature for Ovarian
19 Cancer. *Frontiers in immunology.* 2022;13:951582. doi:10.3389/fimmu.2022.951582
- 20 26. Ding YL, Sun SF, Zhao GL. COL5A2 as a potential clinical biomarker for gastric cancer
21 and renal metastasis. *Medicine.* Feb 19 2021;100(7):e24561.
22 doi:10.1097/md.00000000000024561
- 23 27. Han YL, Luo D, Habaxi K, et al. COL5A2 Inhibits the TGF- β and Wnt/ β -Catenin Signaling
24 Pathways to Inhibit the Invasion and Metastasis of Osteosarcoma. *Frontiers in oncology.*
25 2022;12:813809. doi:10.3389/fonc.2022.813809
- 26 28. Sharp SY, Boxall K, Rowlands M, et al. In vitro biological characterization of a novel,
27 synthetic diaryl pyrazole resorcinol class of heat shock protein 90 inhibitors. *Cancer research.*
28 Mar 1 2007;67(5):2206-16. doi:10.1158/0008-5472.CAN-06-3473

42 13. Supplementary File Legends

43 Supplementary Files

44 **Supplementary File - Figure 1.** Hsa_circ_0000253 centered network.

45 **Supplementary File - Figure 2.** Umap plot of OS cells with 7 clusters.

46 **Supplementary File - Figure 3.** (A) GSEA results of Single-cell transcriptome between hOSC
47 and IOSC. (B) GSEA results of Single-cell transcriptome between OSs and controls.

48 **Supplementary File - Figure 4.** (A) Gene function enrichment analysis results of pink module.
49 (B) Gene function enrichment analysis of yellow module.

50 **Supplementary File - Figure 5.** (A-B) Gene function enrichment analysis results of candidate
51 drug targets based on KEGG database. (C-D) Gene function enrichment analysis results of
52 candidate drug targets based on KEGG database.

53 **Supplementary File - Figure 6.** (A-B) Interaction between CCT-018159 and target protein

1
2
3
4
5
6
7
8
9
10
11
12
13
14
15
16
17
18
19
20
21
22
23
24
25
26
27
28
29
30
31
32
33
34
35
36
37
38
39
40
41
42
43
44
45
46
47
48
49
50
51
52
53
54
55
56
57
58
59
60

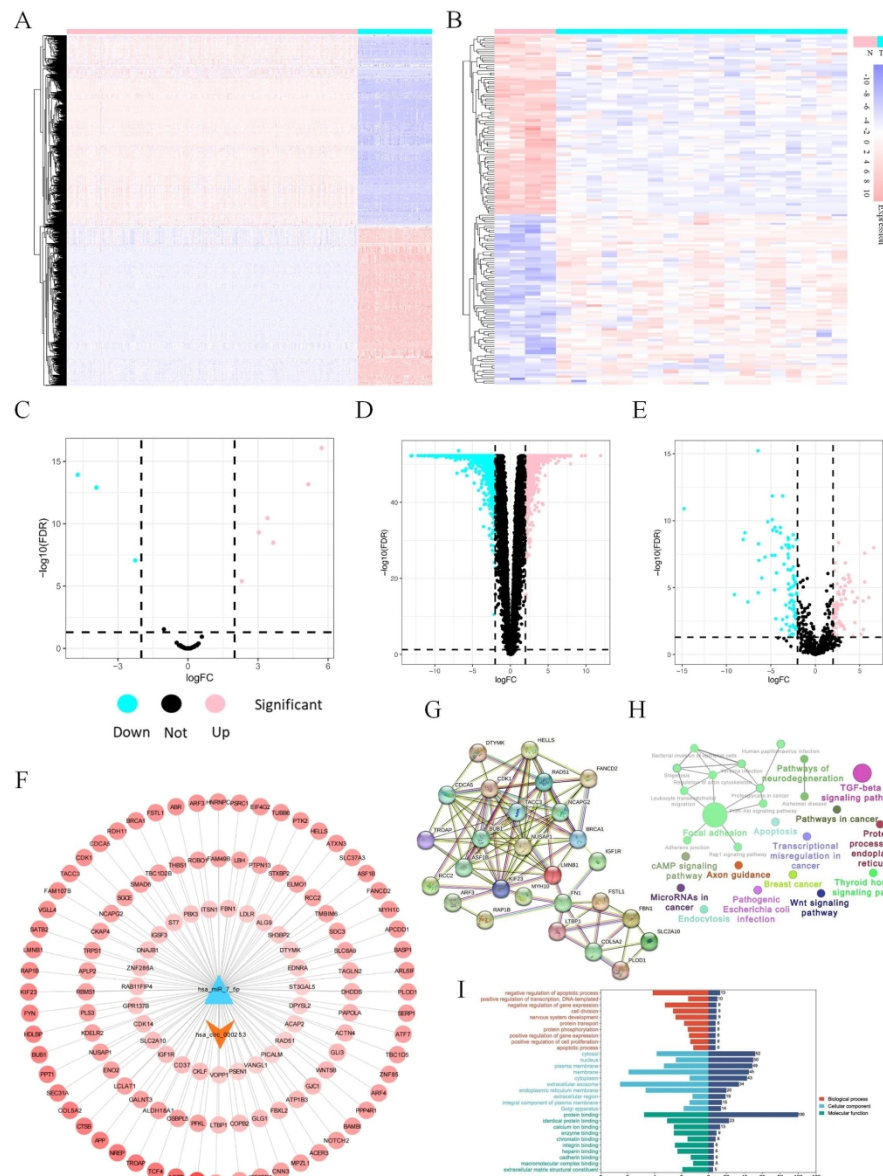
1
2
3 HIF1A at molecular level
4
5

6 **Supplementary File - Table 1.** Forward and reverse primer sequences for RT-qPCR.
7

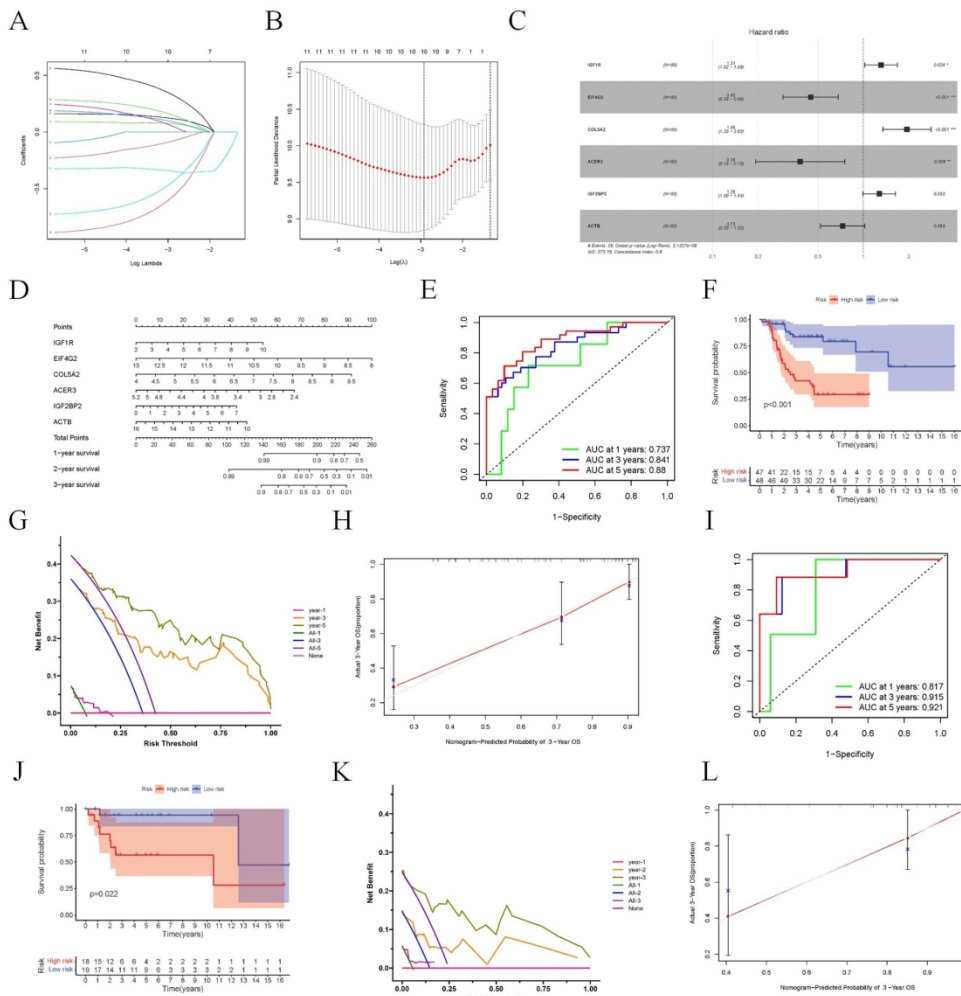
8 **Supplementary File - Table 2.** Results of differential Expression Analysis for circRNA, miRNA
9 and mRNA between OSs and controls.
10

11 **Supplementary File - Table 3.** CMap targeted drug prediction results of genes from pink
12 model in U2OS cell line.
13

14 **Supplementary File - Table 4.** CMap targeted drug prediction results of genes from yellow
15 model in U2OS cell line.
16
17
18
19
20
21
22
23
24
25
26
27
28
29
30
31
32
33
34
35
36
37
38
39
40
41
42
43
44
45
46
47
48
49
50
51
52
53
54
55
56
57
58
59
60

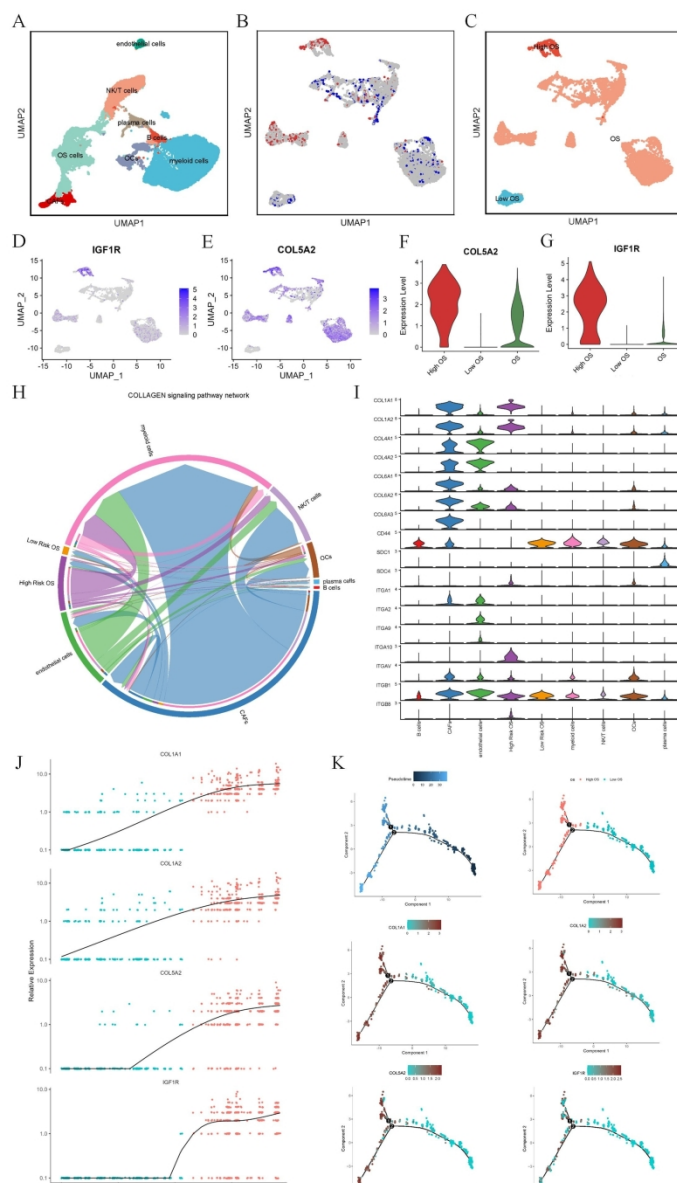


179x235mm (300 x 300 DPI)

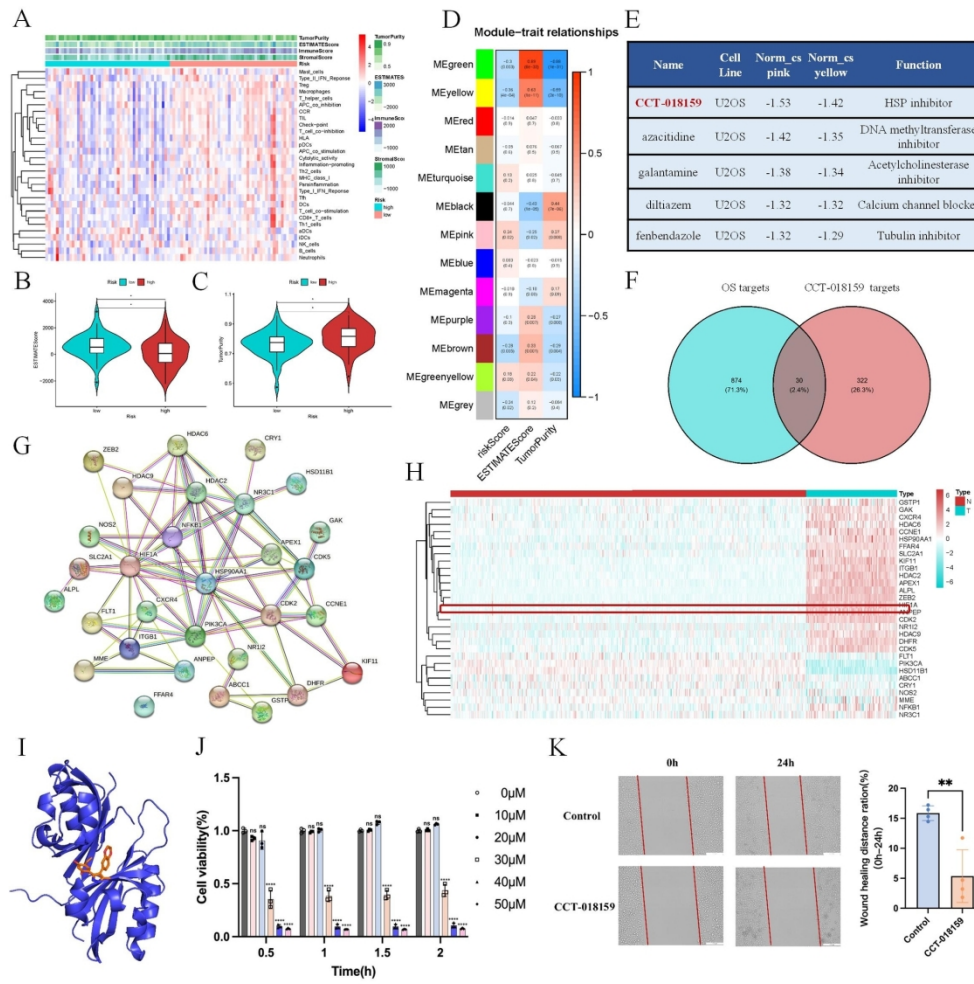


Unable to Convert Image

The dimensions of this image (in pixels) are too large
to be converted. For this image to convert,
the total number of pixels (height x width) must be
less than 40,000,000 (40 megapixels).

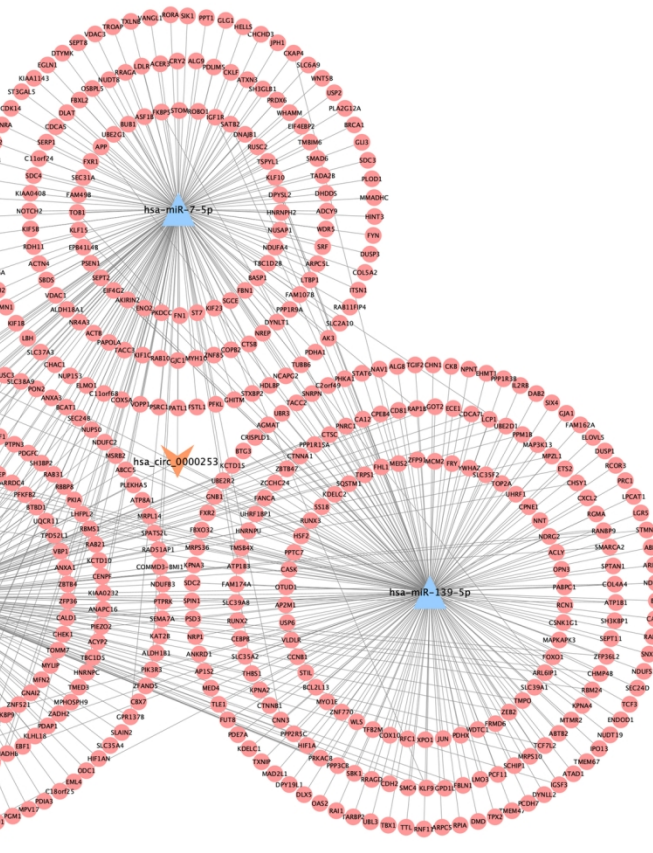


176x306mm (300 x 300 DPI)

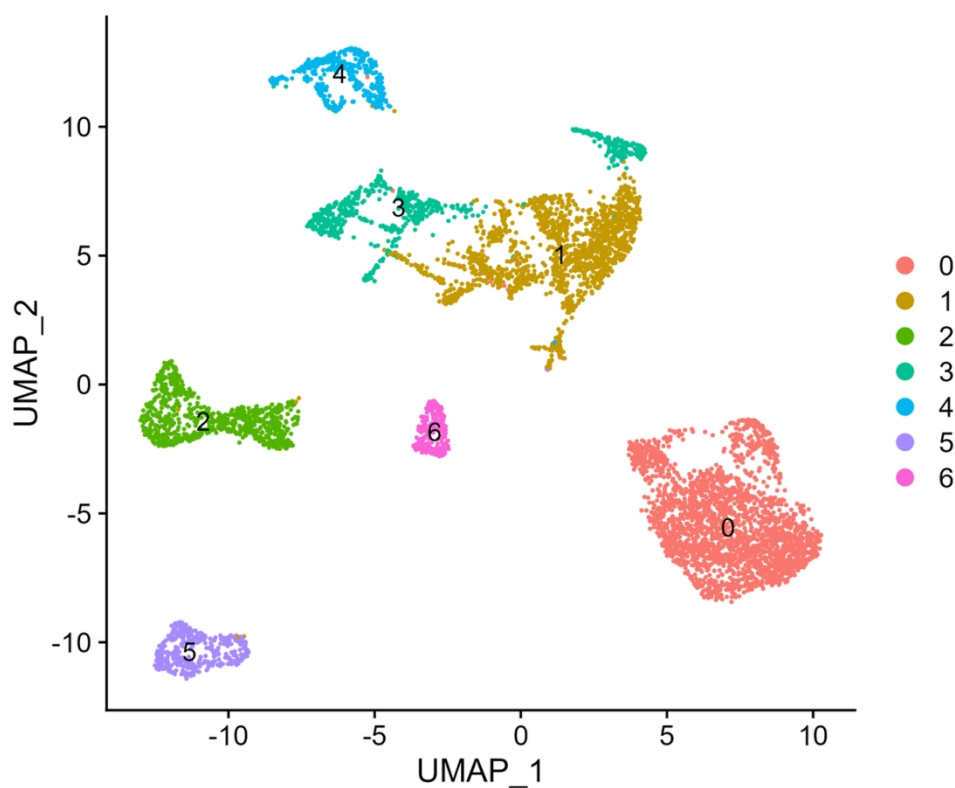


187x187mm (300 x 300 DPI)

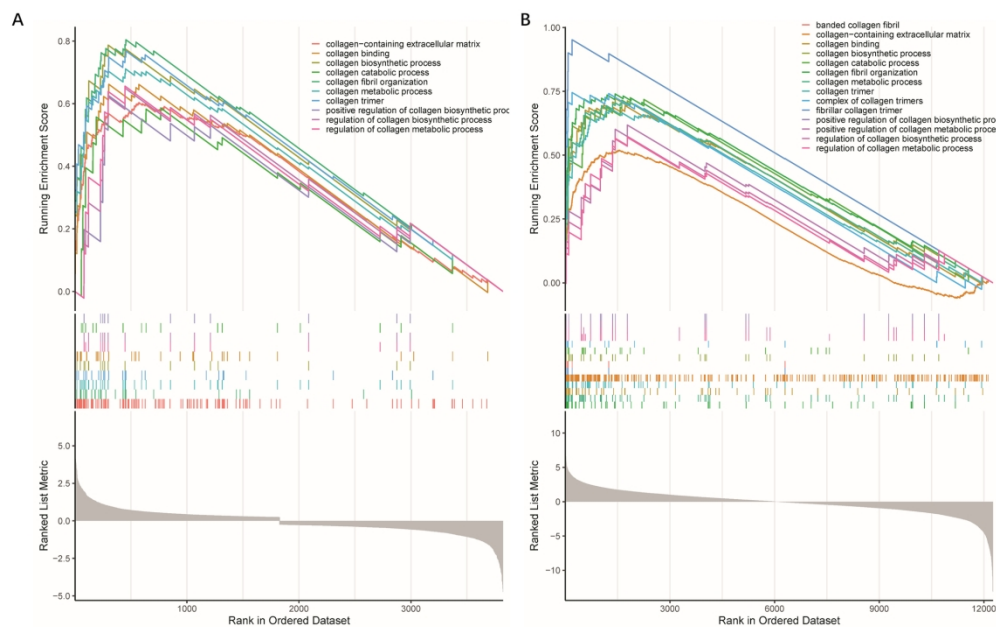
1
2
3
4
5
6
7
8
9
10
11
12
13
14
15
16
17
18
19
20
21
22
23
24
25
26
27
28
29
30
31
32
33
34
35
36
37
38
39
40
41
42
43
44
45
46
47
48
49
50
51
52
53
54
55
56
57
58
59
60



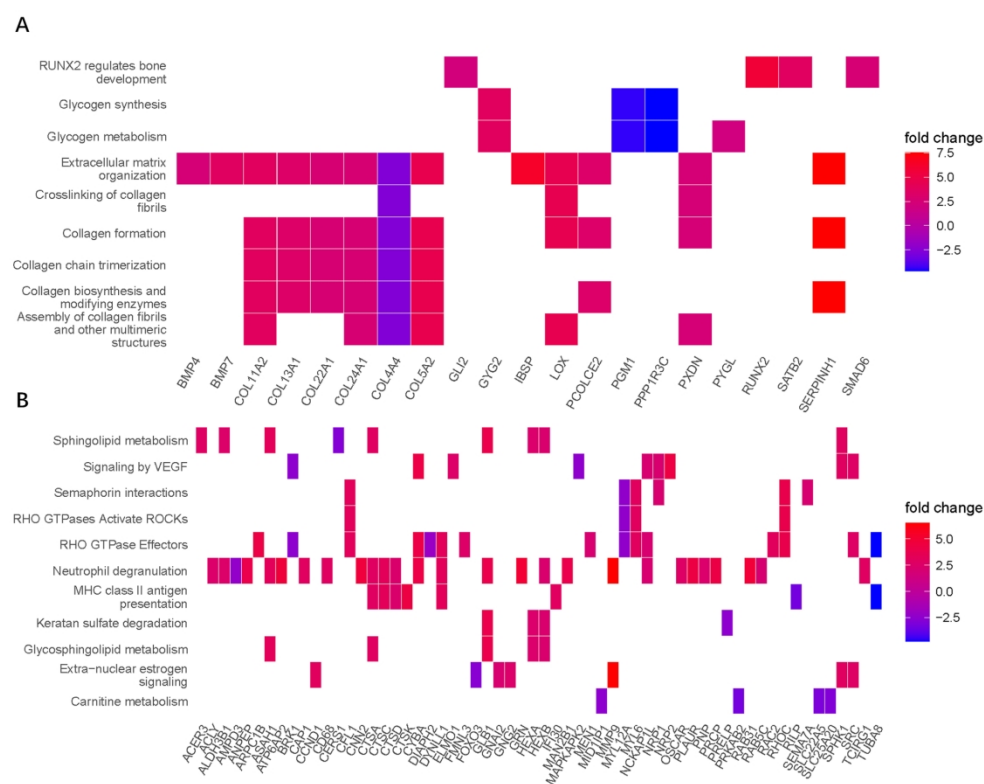
146x127mm (300 x 300 DPI)

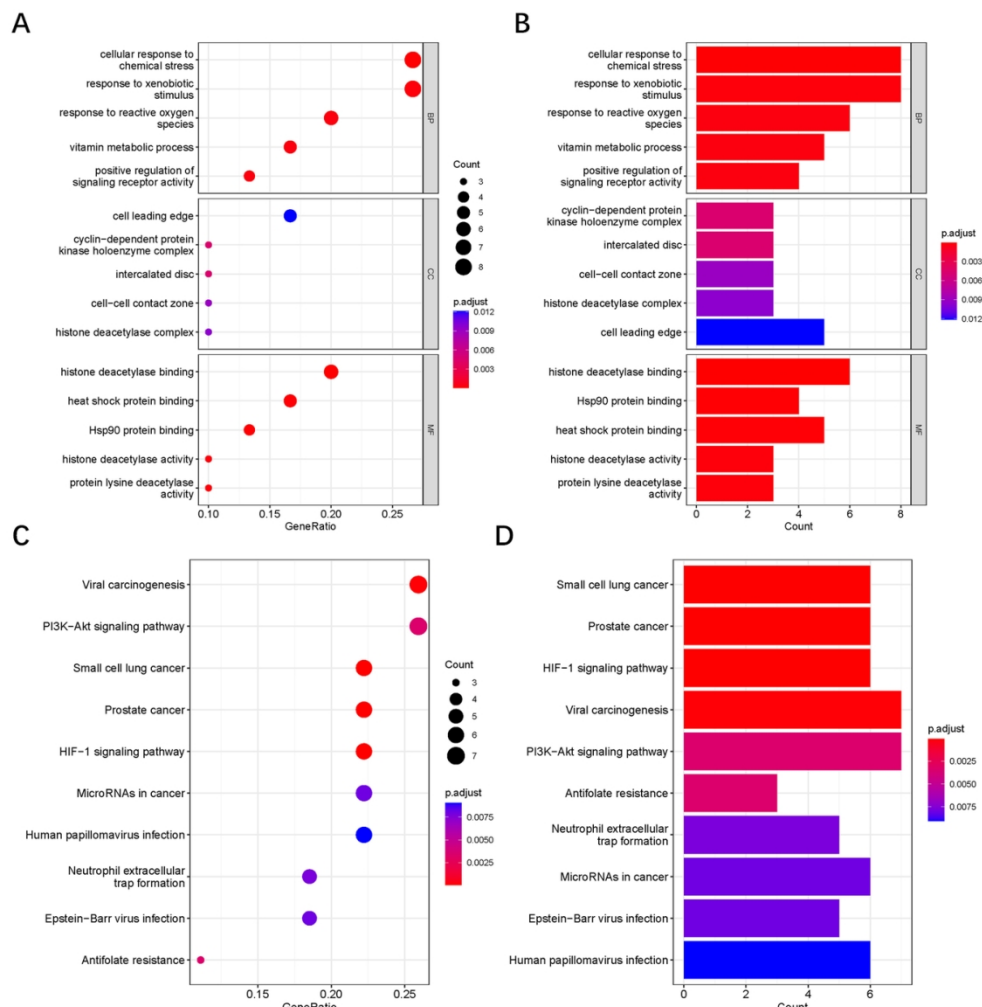


120x100mm (300 x 300 DPI)

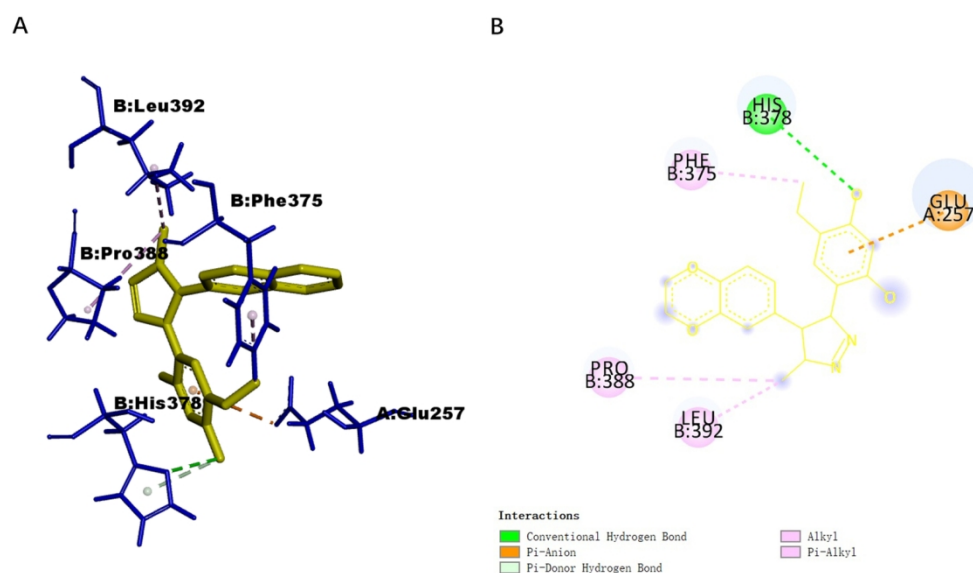


187x118mm (300 x 300 DPI)

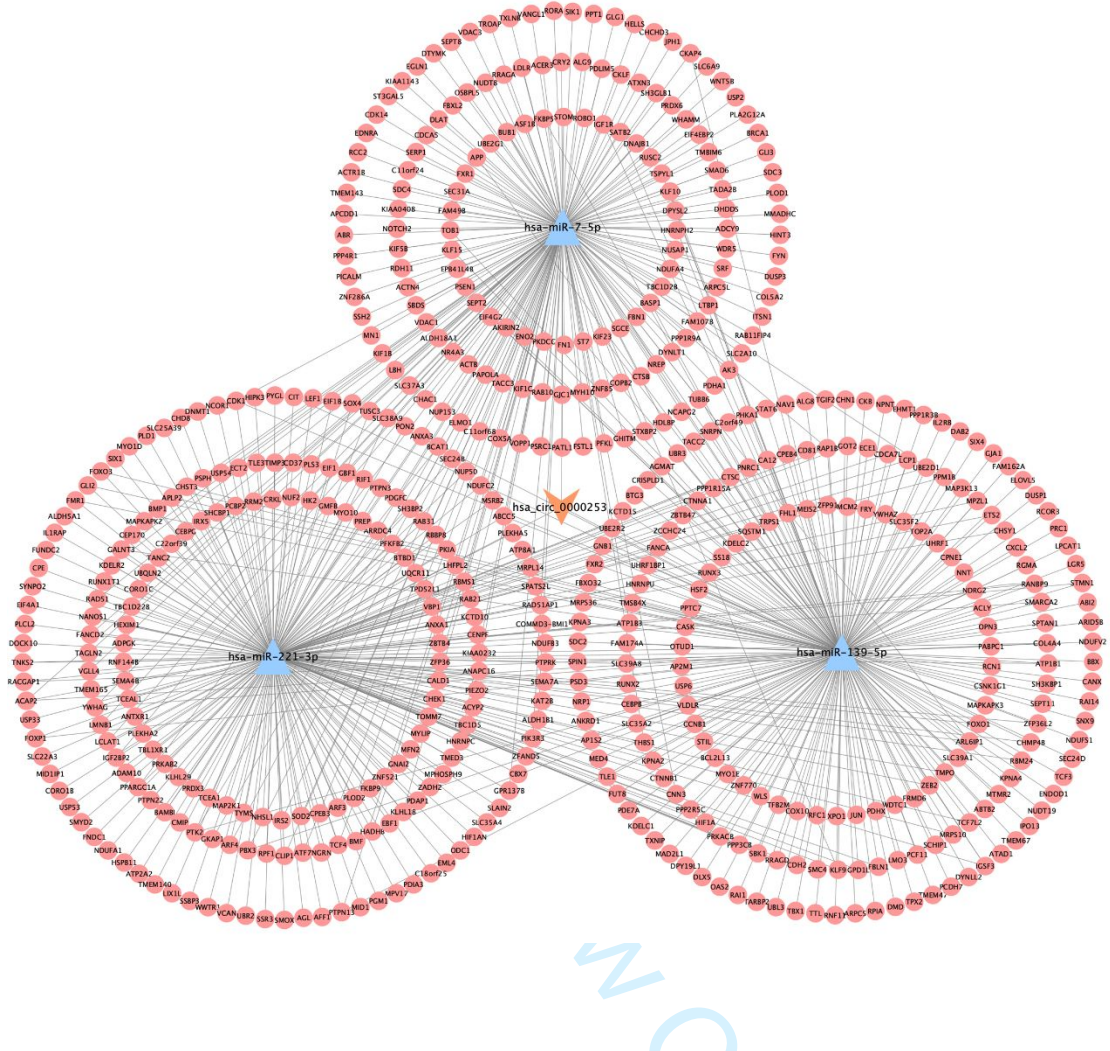




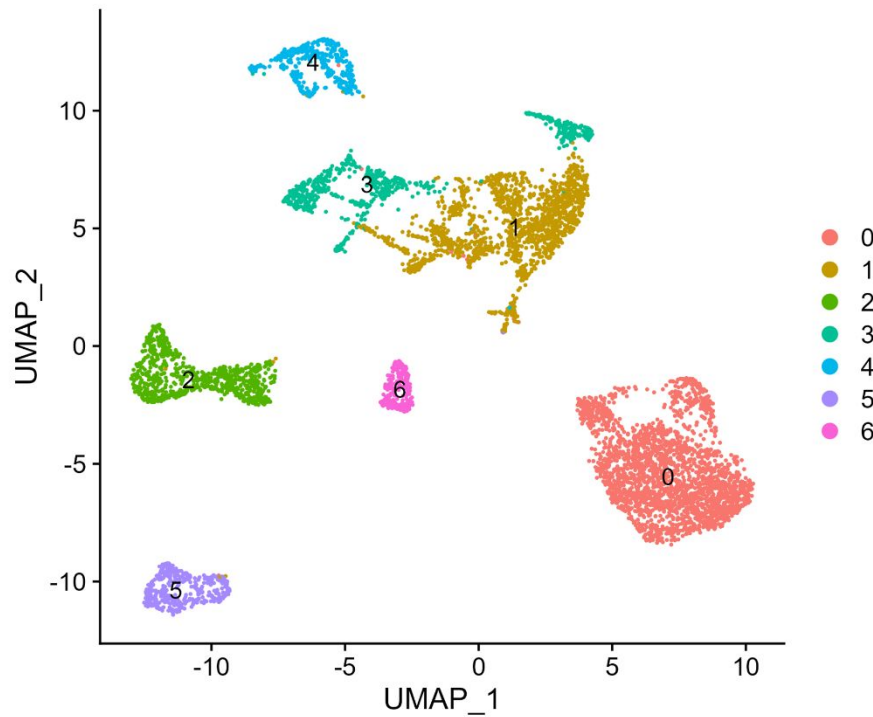
116x119mm (300 x 300 DPI)



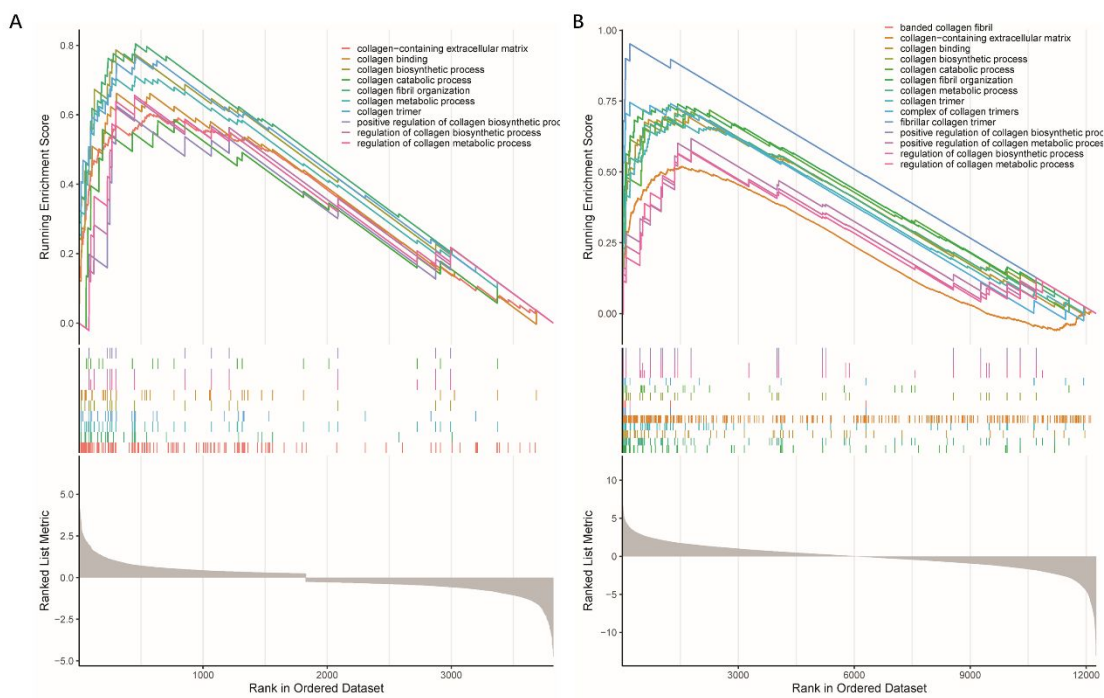
140x88mm (300 x 300 DPI)



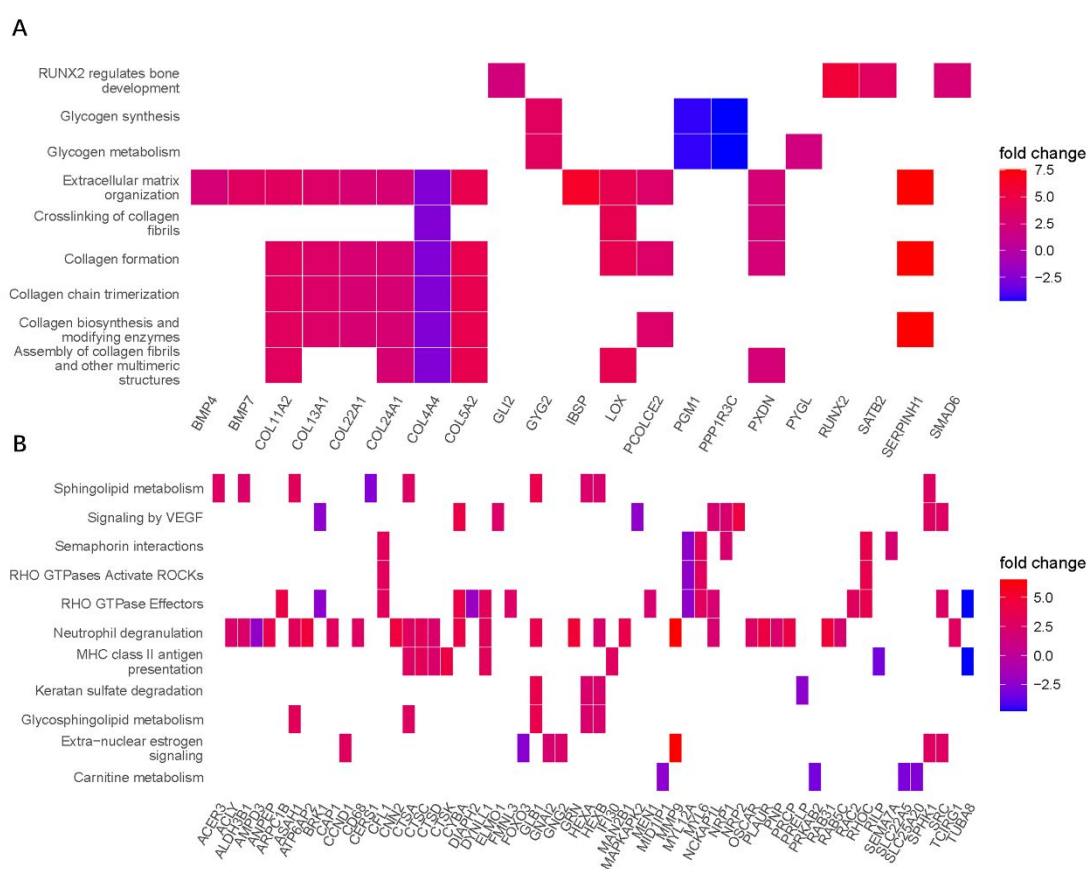
Supplementary File - Figure 1. Hsa_circ_0000253 centered network.



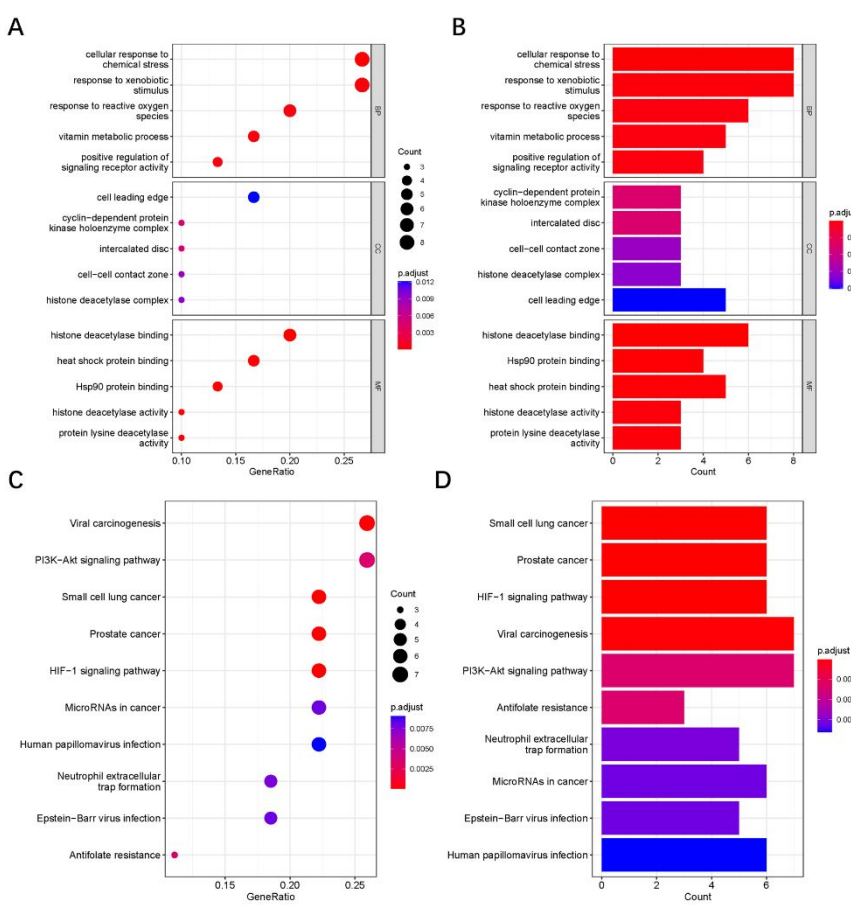
Supplementary File - Figure 2. Umap plot of OS cells with 7 clusters.



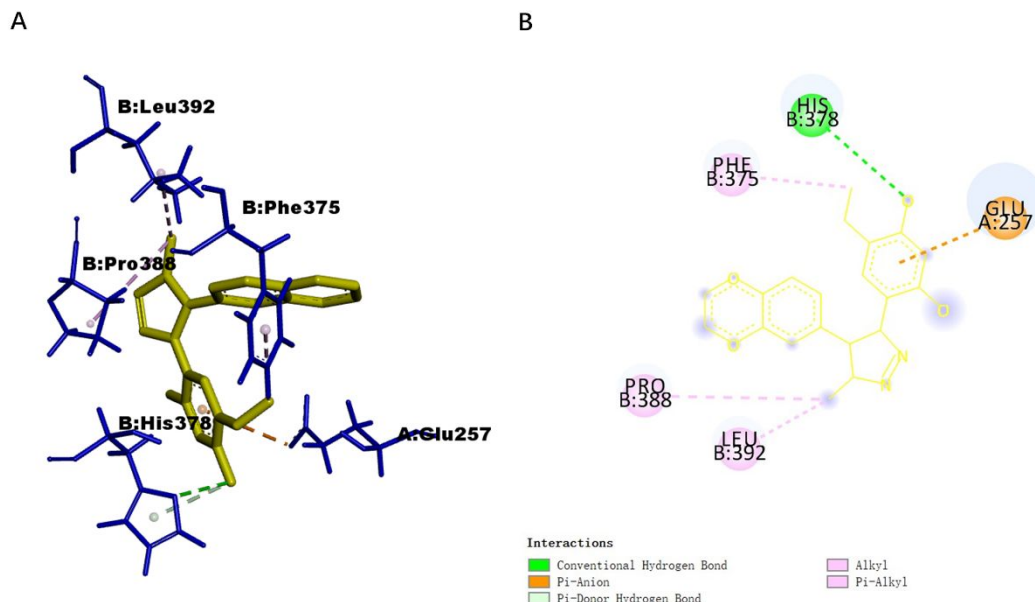
Supplementary File - Figure 3. (A) GSEA results of Single-cell transcriptome between hOSC and IOSC. (B) GSEA results of Single-cell transcriptome between OSs and controls.



Supplementary File - Figure 4. (A) Gene function enrichment analysis results of pink module.
 (B) Gene function enrichment analysis of yellow module.



Supplementary File - Figure 5. (A-B) Gene function enrichment analysis results of candidate drug targets based on KEGG database. (C-D) Gene function enrichment analysis results of candidate drug targets based on KEGG database.



Supplementary File - Figure 6. (A-B) Interaction between CCT-018159 and target protein HIF1A at molecular level

1
2
3 **2. Materials and methods**
4

5 **2.1 Data acquisition and variance analysis**

6 In this experiment, mRNA-seq data was downloaded from the TARGET database
7 (<https://ocg.cancer.gov/programs/target>) and the GTEx database (<https://www.gtexportal.org>).
8 The data included 95 OS samples (from the TARGET database, Jan 2021) and 396 normal
9 tissue samples (from the GTEx database, Jan 2021). The mRNA expression data from both
10 databases were integrated and normalized, the batch effects were removed, and it was then
11 used for subsequent experiments. The clinical information of the OS samples, including age,
12 survival time, and survival status were also downloaded from the TARGET database.
13
14

15
16 The miRNA expression data of OS patients came from the GEO database (GSE28424), which
17 included 19 OS samples and 4 control samples. Additionally, circRNA expression data of OS
18 patients (GSE140256) were obtained from the GEO database, which included 3 OS samples
19 and 3 control samples. We conducted differential analyses of the expression data of these three
20 types of RNA, and drew corresponding volcano plots and heatmaps based on thresholds of
21 $|log_2(\text{fold change, FC})| > 2$ and false discovery rate (FDR) < 0.05 . The removal of batch effects
22 and differential analyses were conducted using the R package 'limma' ¹.
23
24

25 The miRNA-mRNA relationship pairs (screening criteria: Number of Supporting Experiments
26 ≥ 1) and circRNA-miRNA relationship pairs (screening criteria: Number of Supporting
27 Experiments ≥ 2) were obtained from the StarBase v2.0 database ². Then, based on the results
28 of differential analyses, relationship pairs with differential expression at both ends were
29 screened out, and a ceRNA network was constructed based on these pairs. Finally, the circRNA
30 - miRNA - mRNA network was visualized using Cytoscape v.3.7 ³.
31
32

33 **2.2 Establishment and verification of cox risk model**
34

35 We performed a univariate Cox regression analysis on the node genes associated with has-
36 miR-7-5p in the ceRNA network, selected genes with significant differences, and included them
37 in the initial Cox model. To prevent overfitting of the model, we used the least absolute
38 shrinkage selection operator (LASSO) regression model to select genes to build the gene
39 model with the lowest cross-validation point. Subsequently, through the random forest
40 algorithm and multivariate Cox proportional hazard regression, we further screened prognostic
41 markers, plotted the nomogram of patient survival, and divided OS patients into high-risk and
42 low-risk groups based on risk scores. To evaluate the discrimination and accuracy of the
43 nomogram, we respectively plotted the receiver operating characteristic ⁴ and calibration curves
44 for one year, three years, and five years. To validate the obtained prognostic markers, we
45 obtained the external data set GSE39055 from GEO, which includes 37 OS samples as a
46 validation set, and plotted ROC curves, calibration curves, and Decision Curve Analysis (DCA)
47 curves to verify the accuracy of the model. Finally, we plotted Kaplan-Meier survival curves for
48 high and low risk groups based on the original data set and the validation set to judge whether
49 the model has good prognostic value.
50
51

1
2
3 this group of markers can effectively prognosticate.
4
5

6 *2.3 Analysis of Single-Cell Transcriptomics*

7 We downloaded a single-cell data set from the GEO database that includes 6 osteosarcoma
8 samples (GSE162454) (11). We used the Seurat R package (version 4.3.0,
9 <https://github.com/satijalab/seurat>) to filter out cells that had less than 300 and more than 4500
10 genes, and cells with >10% mitochondrial genes. After removing batch effects using Harmony
11 R package (<https://github.com/immunogenomics/Harmony>), we performed a primary cell
12 cluster analysis with a resolution of 0.15 and visualized the clustering results using Uniform
13 Manifold Approximation and Projection (UMAP) dimension reduction analysis. Then, we
14 extracted the OS cells and re-clustered at a resolution of 0.06. The Scissor R package⁵ can
15 determine the phenotype of each cell within a single-cell transcriptome by combining
16 transcriptomic data and classification data of sample phenotypes. Based on Scissor, we
17 predicted the high and low risk phenotypes of OS cells according to the high and low risk
18 features of transcriptome samples generated by the cox risk model, and further identified the
19 high-risk and low-risk OS cell clusters based on the expression level and classification results
20 of validated cell markers (COL5A2 and IGF1R). Finally, we analyzed the communication status
21 of collagen signaling pathway in two types of OS cells using CellChat R package (version 1.6.1)
22 and simulated the development sequence of OS cells using Monocle R package (version
23 2.22.0)⁷.
24
25

32 *2.4 Drug prediction based on network pharmacology*

33 We examined 29 immune-related gene markers and quantitatively assessed the immune
34 activity of the high-risk and low-risk groups using single-sample gene set enrichment analysis
35 (ssGSEA)⁸. We also used the ESTIMATE algorithm⁹ to evaluate the corresponding immun
36 score, stromal score, tumor purity, and ESTIMATE score, and analyzed whether there were
37 differences in these four indicators between the two risk groups. The weighted correlation
38 network analysis (WGCNA)¹⁰ was used to find differentially expressed gene clusters highly
39 correlated with the risk score, immune score, and tumor purity. The expression of two groups
40 of differentially expressed gene clusters screened out by WGCNA was entered into the
41 Connective Map (CMap)¹¹ online server, respectively. From the two drug prediction results, we
42 selected the top 50 drugs in the U2OS cell line and chose the intersection in the two lists.
43 Furthermore, we predicted drug molecular targets through online software PharmMapper¹²⁻¹⁴
44 (<http://lilab-ecust.cn/pharmmapper/index.html>) and SuperPred¹⁵ (<https://prediction.charite.de>),
45 and acquired OS disease targets on the DisGeNET platform¹⁶⁻¹⁹ (<https://www.disgenet.org>)
46 and the Online Mendelian Inheritance in Man platform (OMIM, <https://omim.org>)²⁰. We docked
47 the center target protein with small molecule drugs using software AutoDock Vina^{21,22}.
48
49

56 *2.5 Functional enrichment analysis and PPI network construction*

57 Using the "clusterProfiler" package, we conducted Gene Ontology (GO) and Kyoto
58

1
2
3 Encyclopedia of Genes and Genomes (KEGG) pathway enrichment analysis on differentially
4 expressed network node genes to assess the biological processes (BPs), molecular functions
5 (Mfs), cellular components (CCs), and signal pathways enriched by these genes. The screening
6 criteria was an adjusted P-value of <0.05. The ssGSEA was completed by the R packages
7 "GSVA" and "clusterProfiler" ²³. To study the interaction among genes, a PPI network was
8 constructed through searching the STRING (interaction gene/protein search tool) database
9 (<http://www.string-db.org>) and using the MCODE (Molecular Complex Detection) plugin of the
10 Cytoscape software ²⁴.
11
12
13
14
15

16 *2.6 Cell culture and transfection*

17 The human osteosarcoma cell lines U2OS and MG63 were purchased from Procell Life Science
18 & Technology, Wuhan, China. Cell Line Authentication: Our research involved the utilization of
19 U2OS and MG63 cell lines. The U2OS cell line was acquired in 24th June, 2023, and the MG63
20 cell line was obtained in 18th, July, 2023. U2OS and MG63 cells were cultured in DMEM with
21 10% serum and 1% penicillin/streptomycin antibiotic at 37° C in a 5% CO₂ incubator. The
22 transfection reagents for hsa_circ_0000253, miR7, and COL5A2 were purchased from Ribobio,
23 Guangzhou, and used in a 50 nm system, followed by 48 hours of incubation at 37° C.
24
25
26
27
28

29 *2.7 Detection of cell viability*

30 Cell viability was assessed using the MTT method and CCK-8 method. U2OS cells were
31 seeded in a 96-well plate, with the transfection reagent added to each group, and the
32 absorbance of each well was measured with an enzyme-linked immunoassay reader after 48
33 hours of culture, recording the results. MG-63 cells were seeded in a 96-well plate, with the
34 drug added to each group, and the absorbance of each well was measured with an enzyme-
35 linked immunoassay reader after 0.5, 1, 1.5, 2 hours of culture, recording the results.
36
37
38

39 *2.8 Scratch wound healing assays*

40 U2OS cells were seeded in a 6-well plate. When cell confluence reached 90-100% in the 6-well
41 plate, a linear scratch was made with a 100μL sterile pipette. The cells were incubated with
42 serum-free DMEM. Photos were taken at 0h, 12h, 36h, and 48h with a microscope. The pictures
43 were processed with Photoshop and Image J, calculating the wound healing rate at 0-12h, 12-
44 24h, 24-36h, 36-48h separately. For example, wound healing rate = 1 - (12h wound area / 0h
45 wound area). Statistical analysis was performed with Graphpad Prism v9.0.
46
47
48

49 *2.9 Transwell assays*

50 An 8 μm pore Transwell chamber (LABSELECT, China) was placed in a 24-well plate to test
51 cell migration ability. 500 μL of DMEM with 10% serum was added to the lower chamber, and
52 200 μL cell suspension in serum-free DMEM and transfection reagent was added to the upper
53 chamber. After incubation at 37° C in an incubator for 24 hours, the upper chamber was
54 removed. Cells were washed twice with PBS, and unmigrated cells on the upper layer were
55 removed with a cotton swab. Migrated cells were fixed with 4% paraformaldehyde and stained
56 with 0.5% crystal violet. The number of cells was counted under a microscope.
57
58
59
60

1
2
3 gently removed with a cotton swab. After fixation with 4% paraformaldehyde for 30 min and
4 washing twice with PBS, the migrated cells were stained with 0.1% crystal violet for 60 minutes.
5 The migrated cells were quantified under an inverted fluorescence microscope, with three
6 images taken for each field. Cell number count was performed using Image J v1.0 and the data
7 were analyzed using Graphpad Prism v9.0.
8
9

10
11 **2.10 Western blot analysis**
12

13 The cells were lysed using RIPA buffer (Solaibao, China) in a 100:1 ratio with PMSF to extract
14 protein samples. Protein concentration was determined using BCA protein assay kit (Bioss,
15 China). Sample preparation and Western blot analysis were performed using antibodies against
16 the following proteins: OCT4, SOX2; GAPDH, E-cadherin, β -catenin, collagen I, collagen V
17 (Abclone, China) and HRP conjugated secondary antibody (Lifescience, China). The cells were
18 lysed using RIPA buffer (Solaibao, China) in a 100:1 ratio with PMSF (Solaibao, China) to
19 extract protein samples. Protein concentration was determined using BCA protein assay kit
20 (Bioss, China). Sample preparation and Western blot analysis were performed using antibodies
21 against the following proteins: OCT4, SOX2 (Proteintech, China); GAPDH (Sangon Biotech,
22 China); E-cadherin, β -catenin, Collagen I, Collagen V (Wanleibio, China); HRP conjugated
23 secondary antibody (Beyotime, China).
24
25
26
27
28
29

30 **2.11 Isolation of total RNA and RT-qPCR analysis**
31

32 Total RNA from cells was extracted using TRIzol reagent (Invitrogen, USA). cDNA was
33 synthesized from mRNA using Prime Script RT Master Mix (Takara Biotechnology, Dalian,
34 China) and from circRNA and miRNA using circRNA and miRNA qRT-PCR kit (Ribobio,
35 Guangzhou, China). RT-qPCR was performed using SYBR Premix EX Taq (Takara , Japan),
36 and results were analyzed using the $2^{-\Delta\Delta CT}$ method. All forward and reverse primer sequences
37 can be found in [Supplementary File - Table 1](#).
38
39
40
41
42
43
44
45
46

- 47 1. Ritchie ME, Phipson B, Wu D, et al. limma powers differential expression analyses for
48 RNA-sequencing and microarray studies. *Nucleic acids research*. Apr 20 2015;43(7):e47.
49 doi:10.1093/nar/gkv007
50
51 2. Yang JH, Li JH, Shao P, Zhou H, Chen YQ, Qu LH. starBase: a database for exploring
52 microRNA-mRNA interaction maps from Argonaute CLIP-Seq and Degradome-Seq data.
53 *Nucleic acids research*. Jan 2011;39(Database issue):D202-9. doi:10.1093/nar/gkq1056
54
55 3. Shannon P, Markiel A, Ozier O, et al. Cytoscape: a software environment for integrated
56 models of biomolecular interaction networks. *Genome research*. Nov 2003;13(11):2498-504.
57 doi:10.1101/gr.1239303
58
59 4. The GC, Aguet F, Anand S, et al. The GTEx Consortium atlas of genetic regulatory effects
60 across human tissues. *Science*. 2020/09/11 2020;369(6509):1318-1330.

- 1
2
3 doi:10.1126/science.aaz1776
4 5. Sun D, Guan X, Moran AE, et al. Identifying phenotype-associated subpopulations by
5 integrating bulk and single-cell sequencing data. *Nature biotechnology*. Apr 2022;40(4):527-
6 538. doi:10.1038/s41587-021-01091-3
7 6. Jin S, Guerrero-Juarez CF, Zhang L, et al. Inference and analysis of cell-cell
8 communication using CellChat. *Nature communications*. Feb 17 2021;12(1):1088.
9 doi:10.1038/s41467-021-21246-9
10 7. Qiu X, Hill A, Packer J, Lin D, Ma YA, Trapnell C. Single-cell mRNA quantification and
11 differential analysis with Census. *Nature methods*. Mar 2017;14(3):309-315.
12 doi:10.1038/nmeth.4150
13 8. Hänelmann S, Castelo R, Guinney J. GSVA: gene set variation analysis for microarray
14 and RNA-seq data. *BMC bioinformatics*. Jan 16 2013;14:7. doi:10.1186/1471-2105-14-7
15 9. Yoshihara K, Shahmoradgoli M, Martínez E, et al. Inferring tumour purity and stromal and
16 immune cell admixture from expression data. *Nature communications*. 2013;4:2612.
17 doi:10.1038/ncomms3612
18 10. Langfelder P, Horvath S. WGCNA: an R package for weighted correlation network analysis.
19 *BMC bioinformatics*. Dec 29 2008;9:559. doi:10.1186/1471-2105-9-559
20 11. Lamb J, Crawford ED, Peck D, et al. The Connectivity Map: using gene-expression
21 signatures to connect small molecules, genes, and disease. *Science (New York, NY)*. Sep 29
22 2006;313(5795):1929-35. doi:10.1126/science.1132939
23 12. Wang X, Shen Y, Wang S, et al. PharmMapper 2017 update: a web server for potential
24 drug target identification with a comprehensive target pharmacophore database. *Nucleic acids
25 research*. Jul 3 2017;45(W1):W356-w360. doi:10.1093/nar/gkx374
26 13. Liu X, Ouyang S, Yu B, et al. PharmMapper server: a web server for potential drug target
27 identification using pharmacophore mapping approach. *Nucleic acids research*. Jul
28 2010;38(Web Server issue):W609-14. doi:10.1093/nar/gkq300
29 14. Wang X, Pan C, Gong J, Liu X, Li H. Enhancing the Enrichment of Pharmacophore-Based
30 Target Prediction for the Polypharmacological Profiles of Drugs. *Journal of chemical
31 information and modeling*. Jun 27 2016;56(6):1175-83. doi:10.1021/acs.jcim.5b00690
32 15. Gallo K, Goede A, Preissner R, Gohlke BO. SuperPred 3.0: drug classification and target
33 prediction-a machine learning approach. *Nucleic acids research*. Jul 5 2022;50(W1):W726-
34 w731. doi:10.1093/nar/gkac297
35 16. Piñero J, Bravo À, Queralt-Rosinach N, et al. DisGeNET: a comprehensive platform
36 integrating information on human disease-associated genes and variants. *Nucleic acids
37 research*. 2017;45(D1):D833-D839. doi:10.1093/nar/gkw943
38 17. Piñero J, Queralt-Rosinach N, Bravo À, et al. DisGeNET: a discovery platform for the
39 dynamical exploration of human diseases and their genes. *Database : the journal of biological
40 databases and curation*. 2015;2015:bav028. doi:10.1093/database/bav028
41 18. Piñero J, Ramírez-Anguita JM, Saüch-Pitarch J, et al. The DisGeNET knowledge platform
42 for disease genomics: 2019 update. *Nucleic acids research*. 2020;48(D1):D845-D855.
43 doi:10.1093/nar/gkz1021
44 19. Piñero J, Saüch J, Sanz F, Furlong LI. The DisGeNET cytoscape app: Exploring and
45 visualizing disease genomics data. *Computational and Structural Biotechnology Journal*.
46 2021/01/01/ 2021;19:2960-2967. doi:<https://doi.org/10.1016/j.csbj.2021.05.015>

- 1
2
3
4
5
6
7
8
9
10
11
12
13
14
15
16
17
18
19
20
21
22
23
24
25
26
27
28
29
30
31
32
33
34
35
36
37
38
39
40
41
42
43
44
45
46
47
48
49
50
51
52
53
54
55
56
57
58
59
60
20. Amberger JS, Bocchini CA, Schiettecatte F, Scott AF, Hamosh A. OMIM.org: Online Mendelian Inheritance in Man (OMIM®), an online catalog of human genes and genetic disorders. *Nucleic acids research*. Jan 2015;43(Database issue):D789-98. doi:10.1093/nar/gku1205
21. Eberhardt J, Santos-Martins D, Tillack AF, Forli S. AutoDock Vina 1.2.0: New Docking Methods, Expanded Force Field, and Python Bindings. *Journal of chemical information and modeling*. 2021/08/23 2021;61(8):3891-3898. doi:10.1021/acs.jcim.1c00203
22. Trott O, Olson AJ. AutoDock Vina: Improving the speed and accuracy of docking with a new scoring function, efficient optimization, and multithreading. 2010;31(2):455-461. doi:<https://doi.org/10.1002/jcc.21334>
23. Wu T, Hu E, Xu S, et al. clusterProfiler 4.0: A universal enrichment tool for interpreting omics data. *Innovation (Cambridge (Mass))*. Aug 28 2021;2(3):100141. doi:10.1016/j.xinn.2021.100141
24. Yin H, Wang S, Gu C. Identification of Molecular Signatures in Mild Intrinsic Atopic Dermatitis by Bioinformatics Analysis. *Annals of dermatology*. Apr 2020;32(2):130-140. doi:10.5021/ad.2020.32.2.130
- For Review Only

Supplementary File - Table 1. Forward and reverse primer sequences for RT-qPCR.

| Genes | F | R |
|--------------|----------------------------|--------------------------|
| circ_0000253 | TGCAATGGTGGGAAATCAGTG | ACAGCAGGTACCATGTTGTGCTA |
| COL5A2 | GACTGTGCCGACCCCTGTAAC | CCTGGACGACCACGTATGC |
| miR-7 | GCGCGTGGAAGACTAGTGATT | AGTGCAGGGTCCGAGGTATT |
| MKI67 | CCATGAGAACAGAGGCAGCAAGAAGG | GGAAGTCCAAGAGCAAGGTGTCAG |
| GAPDH | CCCAGCCACATACCAGGAAATGAG | GACTTCAACAGCGACACCCACTC |

1
2
3 **Supplementary File - Table 2.** Results of differential Expression Analysis for circRNA, miRNA
4 and mRNA between OSs and controls.
5

| id | logFC | Average Expression | t | P value | Adjusted P value | B |
|------------------|----------|--------------------|----------|----------|------------------|----------|
| hsa_circ_0000006 | -5.7264 | -2.14377 | 23.94773 | 1.01E-18 | 8.45E-17 | 32.73644 |
| hsa_circ_0010220 | 4.720786 | 0.993151 | -18.8792 | 2.80E-16 | 1.17E-14 | 27.29621 |
| hsa_circ_0046264 | -5.15134 | -2.11156 | 17.19427 | 2.45E-15 | 6.86E-14 | 25.15985 |
| hsa_circ_0000253 | 3.918484 | 0.71517 | -16.5424 | 5.96E-15 | 1.25E-13 | 24.28023 |
| hsa_circ_0078767 | -3.40819 | -1.36359 | 12.73602 | 2.07E-12 | 3.47E-11 | 18.4365 |
| hsa_circ_0094088 | -3.03195 | -1.35236 | 11.14836 | 3.54E-11 | 4.96E-10 | 15.57416 |
| hsa_circ_0096041 | -3.6524 | -1.79496 | 10.08617 | 2.78E-10 | 3.33E-09 | 13.49336 |
| hsa_circ_0020378 | 2.257567 | 0.525775 | -8.47241 | 8.31E-09 | 8.73E-08 | 10.05421 |
| hsa_circ_0049271 | -2.30559 | 0.024326 | 6.773358 | 4.30E-07 | 4.02E-06 | 6.063143 |

For Review Only

Supplementary File - Table 3. CMap targeted drug prediction results of genes from pink model in U2OS cell line.

| ID | Perturbation identifier | Perturbation name | Perturbation dose | Perturbation time | Number of samples | Signature size in genes | Connectivity score at the 75th percentile | Treatment activity score | Quality control pass | High quality | Mechanism of action | Target name | Raw connectivity score | False discovery rate q-value | Normalized connectivity score |
|---|-------------------------|-------------------|-------------------|-------------------|-------------------|-------------------------|---|--------------------------|----------------------|--------------|---|---|------------------------|------------------------------|-------------------------------|
| ASG003_U2OS_6H:F18 | BRD-A71390734 | idarubicin | 0.12 uM | 6 h | 5 | 346 | 0.52 | 0.43 | 0 | 0 | Topoisomerase inhibitor | TOP2A | -0.47 | 15.65 | -1.76 |
| LKCP002_U2OS_24H:P18 | BRD-K91966436 | daunorubicin | 0.12 uM | 24 h | 5 | 633 | 0.66 | 0.65 | 1 | 1 | -666 | -666 | -0.43 | 1.39 | -1.59 |
| PAC005_U2OS_6H:BRD-A67514145-003-03-3:5.544 | BRD-A67514145 | furladtadone | 6.66 uM | 6 h | 2 | 46 | 0.16 | 0.09 | 1 | 0 | Bacterial DNA inhibitor | -666 | -0.43 | 1.39 | -1.58 |
| PAC004_U2OS_6H:BRD-K12968785-001-02:6:10 | BRD-K12968785 | bergapten | 10 uM | 6 h | 2 | 56 | 0.39 | 0.15 | 1 | 1 | -666 | -666 | -0.43 | 1.39 | -1.58 |
| PAC004_U2OS_6H:BRD-K11163873-001-02-8:25.6126 | BRD-K11163873 | phenanthridone | 25 uM | 6 h | 2 | 21 | 0.05 | 0.03 | 1 | 0 | PARP inhibitor | PARP1 | -0.42 | 1.39 | -1.55 |
| PAC005_U2OS_6H:BRD-A66199457-001-02-2:2.08524 | BRD-A66199457 | asiaticoside | 2.22 uM | 6 h | 2 | 74 | 0.17 | 0.11 | 1 | 0 | Carcinogen | -666 | -0.41 | 1.39 | -1.53 |
| PAC001_U2OS_6H:BRD-K65503129-001-01:4:10 | BRD-K65503129 | CCT-018159 | 10 uM | 6 h | 2 | 97 | 0.42 | 0.2 | 0 | 0 | HSP inhibitor | HSP90AA1 HSP90AB1 | -0.41 | 1.39 | -1.53 |
| PAC001_U2OS_6H:BRD-K66295376-001-02:4:10 | BRD-K66295376 | ferulic-acid | 10 uM | 6 h | 2 | 41 | 0.05 | 0.05 | 0 | 0 | Antioxidant | CA1 CA12 CA14 CA2 CA4 CA6 CA9 | -0.41 | 1.39 | -1.52 |
| TA.OE005_U2OS_72H:BRDN0000464852:1 | BRDN0000464852 | YAP1 | 1.0 uL | 72 h | 2 | 96 | 0.19 | 0.14 | 1 | 1 | -666 | -666 | -0.4 | 1.39 | -1.49 |
| PAC001_U2OS_6H:BRD-K71799778-001-02:2:10 | BRD-K71799778 | BML-259 | 10 uM | 6 h | 2 | 239 | 0.58 | 0.38 | 0 | 0 | CDK inhibitor | CDK2 CDK5 | -0.4 | 1.39 | -1.49 |
| ASG003_U2OS_6H:O21 | BRD-A37630846 | daunorubicin | 0.12 uM | 6 h | 5 | 373 | 0.57 | 0.47 | 0 | 0 | RNA synthesis inhibitor Topoisomerase inhibitor | TOP2A TOP2B | -0.4 | 1.05 | -1.48 |
| PAC001_U2OS_6H:BRD-K64236792-002-03:2:7.1348 | BRD-K64236792 | austricine | 6.66 uM | 6 h | 2 | 27 | 0.14 | 0.06 | 0 | 0 | -666 | -666 | -0.4 | 0.93 | -1.47 |
| LKCP002_U2OS_24H:N16 | BRD-K12906202 | carbendazim | 10 uM | 24 h | 5 | 162 | 0.21 | 0.19 | 1 | 1 | Tubulin inhibitor | TP53 TUBB | -0.4 | 0.94 | -1.47 |
| PAC003_U2OS_6H:BRD-K26997899-001-01:4:10 | BRD-K26997899 | D-64131 | 10 uM | 6 h | 2 | 85 | 0.48 | 0.2 | 1 | 1 | Tubulin inhibitor | TUBB | -0.4 | 1.04 | -1.47 |
| PAC002_U2OS_6H:BRD-K41567533-001-02:6:10 | BRD-K41567533 | coumophos | 10 uM | 6 h | 2 | 205 | 0.41 | 0.29 | 0 | 0 | Cholinesterase inhibitor | -666 | -0.39 | 0.91 | -1.46 |
| ASG003_U2OS_48H:B10 | BRD-K47832606 | flouxuridine | 10 uM | 48 h | 5 | 194 | 0.44 | 0.3 | 1 | 1 | DNA synthesis inhibitor | TYMS | -0.4 | 0.91 | -1.46 |
| TA.OE005_U2OS_72H:BRDN0000464873:1 | BRDN0000464873 | PPARGC1A | 1.0 uL | 72 h | 2 | 281 | 0.42 | 0.35 | 1 | 1 | -666 | -666 | -0.39 | 0.82 | -1.45 |
| PAC001_U2OS_6H:BRD-K77641333-003-04:0:10 | BRD-K77641333 | naphazoline | 10 uM | 6 h | 2 | 47 | 0.13 | 0.08 | 0 | 0 | Adrenergic receptor agonist | ADRA1A ADRA2A | -0.39 | 0.71 | -1.43 |
| LKCP001_U2OS_48H:M22 | BRD-K74065929 | doramapimod | 10 uM | 48 h | 5 | 355 | 0.48 | 0.42 | 1 | 1 | P38 MAPK inhibitor | MAPK14 MAPK11 MAPK12 DDR2 MAPK13 | -0.39 | 0.71 | -1.43 |
| TAK004_U2OS_96H:TRCN0000221543:1 | TRCN0000221543 | MTOR | 1 uL | 96 h | 3 | 122 | 0.38 | 0.22 | 0 | 0 | -666 | -666 | -0.39 | 0.71 | -1.43 |
| LKCP002_U2OS_24H:O10 | BRD-K55026842 | azacitidine | 10 uM | 24 h | 5 | 454 | 0.56 | 0.51 | 0 | 0 | DNA methyltransferase inhibitor | DNMT1 DNMT3A | -0.38 | 0.69 | -1.42 |
| PAC003_U2OS_6H:BRD-K37798499-001-02:5:3.39814 | BRD-K37798499 | etoposide | 3.33 uM | 6 h | 2 | 111 | 0.41 | 0.22 | 1 | 1 | Topoisomerase inhibitor | TOP2A TOP2B CYP2E1 CYP3A5 | -0.38 | 0.69 | -1.42 |
| PAC005_U2OS_6H:BRD-A55756846-001-05:5:17.1604 | BRD-A55756846 | H-7 | 15 uM | 6 h | 2 | 305 | 0.45 | 0.37 | 1 | 1 | PKA inhibitor | -666 | -0.38 | 0.69 | -1.42 |
| LKCP001_U2OS_48H:P07 | BRD-K07572174 | curcumin | 10 uM | 48 h | 5 | 576 | 0.64 | 0.61 | 1 | 1 | Cyclooxygenase inhibitor | PTGS1 PTGS2 CCND1 DNMT1 GGPC MAPT APP CA1 CA12 CA14 CA2 CA4 | -0.38 | 0.69 | -1.42 |

| | | | | | | | | | | | | | | | |
|---|----------------|------------------|---------|------|---|-----|------|------|---|---|--|---|-------|------|-------|
| | | | | | | | | | | Histone acetyltransferase inhibitor Lipoxygenase inhibitor NFkB inhibitor | CA6 CA9 CYP3A4 DNMT3B EP300 MMP13 MMP9 NOS2 XDH | | | | |
| PAC069_U2OS_6H:BRD-K61993165-001-06:5:20 | BRD-K61993165 | niacin | 20 uM | 6 h | 3 | 53 | 0.2 | 0.1 | 1 | 1 | -666 | -666 | -0.38 | 0.69 | -1.39 |
| PAC002_U2OS_6H:BRD-K48059230-003-01:1:10 | BRD-K48059230 | YM-298198 | 10 uM | 6 h | 2 | 51 | 0.02 | 0.03 | 0 | 0 | Glutamate receptor antagonist | -666 | -0.38 | 0.69 | -1.39 |
| TA.OE005_U2OS_72H:BRDN000464855:1 | BRDN000464855 | CSNK1A1 | 1.0 uL | 72 h | 2 | 89 | 0.13 | 0.11 | 1 | 0 | -666 | -666 | -0.38 | 0.69 | -1.39 |
| LKCP001_U2OS_48H:P19 | BRD-K16730910 | regorafenib | 10 uM | 48 h | 5 | 560 | 0.56 | 0.57 | 1 | 1 | FGFR inhibitor KIT inhibitor PDGFR inhibitor RAF inhibitor RET inhibitor VEGFR inhibitor | KDR KIT RET FLT1 FLT4 PDGFRA TEK BRAF ABL1 DDR2 FGFR1 FGFR2 FRK MAPK11 PDGFRB RAF1 CYP2B6 CYP2C19 CYP2C8 FGF2 EPHA2 NTRK1 | -0.38 | 0.69 | -1.39 |
| PAC001_U2OS_6H:BRD-K66353228-001-05:4-11.8638 | BRD-K66353228 | zoxazolamine | 12 uM | 6 h | 2 | 100 | 0.16 | 0.13 | 0 | 0 | Muscle relaxant | -666 | -0.37 | 0.64 | -1.38 |
| PAC002_U2OS_6H:BRD-K49481516-004-03:5:10 | BRD-K49481516 | galantamine | 10 uM | 6 h | 2 | 185 | 0.48 | 0.3 | 0 | 0 | Acetylcholinesterase inhibitor | ACHE BCHE CHRNA1 CHRNA10 CHRNA2 CHRNA3 CHRNA4 CHRNA5 CHRNA6 CHRNA7 CHRNA9 CHRN81 CHRN82 CHRN83 CHRN84 CHRN85 CHRNE CHRN9G | -0.37 | 0.66 | -1.38 |
| MOA001_U2OS_24H:N20 | BRD-K30874624 | K-252A | 0.37 uM | 24 h | 2 | 163 | 0.44 | 0.27 | 1 | 1 | -666 | -666 | -0.37 | 0.57 | -1.36 |
| PAC002_U2OS_6H:BRD-K60184833-001-02:3:10 | BRD-K60184833 | TYRPHOSTIN-46 | 10 uM | 6 h | 2 | 83 | 0.21 | 0.13 | 0 | 0 | Tyrosine kinase inhibitor | EGFR | -0.37 | 0.57 | -1.36 |
| PAC001_U2OS_6H:BRD-K72462751-001-01:9:10 | BRD-K72462751 | C-1 | 10 uM | 6 h | 2 | 88 | 0.35 | 0.18 | 0 | 0 | Protein kinase inhibitor | PRKCA | -0.36 | 0.54 | -1.35 |
| PAC005_U2OS_6H:BRD-A65051990-001-03:8:5.6605 | BRD-A65051990 | acenocoumarol | 6.66 uM | 6 h | 2 | 37 | 0.12 | 0.07 | 1 | 0 | Vitamin K antagonist | VKORC1 | -0.37 | 0.57 | -1.35 |
| ASG003_U2OS_24H:H19 | BRD-K37890730 | camptothecin | 10 uM | 24 h | 5 | 482 | 0.7 | 0.59 | 0 | 0 | Topoisomerase inhibitor | TOP1 HIF1A | -0.36 | 0.54 | -1.34 |
| TAK004_U2OS_96H:TRCN0000271642:1 | TRCN0000271642 | GRB10 | 1 uL | 96 h | 3 | 97 | 0.2 | 0.14 | 0 | 0 | -666 | -666 | -0.36 | 0.54 | -1.34 |
| LKCP002_U2OS_24H:I19 | BRD-K24844714 | fluorouracil | 10 uM | 24 h | 5 | 298 | 0.4 | 0.35 | 1 | 1 | Thymidylate synthase inhibitor | -666 | -0.36 | 0.54 | -1.34 |
| PAC004_U2OS_6H:BRD-K12219985-001-04:8-11.2225 | BRD-K12219985 | glipizide | 12 uM | 6 h | 2 | 17 | 0.26 | 0.07 | 0 | 0 | Sulfonylurea | ABC8 KCNJ11 KCNJ10 PPARG | -0.36 | 0.54 | -1.34 |
| TA.OE005_U2OS_72H:BRDN000404512:1 | BRDN000404512 | MOS | 1.0 uL | 72 h | 2 | 80 | 0.05 | 0.07 | 1 | 0 | -666 | -666 | -0.36 | 0.51 | -1.33 |
| PAC005_U2OS_6H:BRD-A74904029-001-04:0-15.6671 | BRD-A74904029 | EI-231 | 15 uM | 6 h | 2 | 407 | 0.16 | 0.26 | 1 | 1 | Casein kinase inhibitor | CSNK2A1 | -0.36 | 0.51 | -1.33 |
| TA.OE005_U2OS_72H:BRDN000464853:1 | BRDN000464853 | APC | 1.0 uL | 72 h | 2 | 203 | 0.14 | 0.17 | 0 | 0 | -666 | -666 | -0.36 | 0.52 | -1.33 |
| PAC003_U2OS_6H:BRD-K27062708-001-04:1:10 | BRD-K27062708 | chlorotriานisene | 10 uM | 6 h | 2 | 14 | 0.25 | 0.06 | 1 | 0 | Estrogenic hormone | ESR1 ESR2 | -0.36 | 0.54 | -1.33 |
| LKCP002_U2OS_6H:D22 | BRD-K51318897 | fenbendazole | 10 uM | 6 h | 4 | 353 | 0.53 | 0.44 | 1 | 1 | Tubulin inhibitor | CYP2C19 CYP2D6 CYP2J2 CYP3A4 TUBB | -0.36 | 0.46 | -1.32 |
| PAC001_U2OS_6H:BRD-K71198913-001-02:3:1 | BRD-K71198913 | 2-AG | 1.11 uM | 6 h | 2 | 62 | 0.25 | 0.13 | 0 | 0 | -666 | -666 | -0.36 | 0.46 | -1.32 |
| PAC003_U2OS_6H:BRD-K24023109-001-02:5:12.0622 | BRD-K24023109 | diltiazem | 12 uM | 6 h | 2 | 81 | 0.1 | 0.09 | 1 | 0 | Calcium channel blocker | CACNA1C CYP3A5 CYP3A7 CACNA1S CACNA2D1 CACNG1 HTR3A KCNQ5 | -0.36 | 0.47 | -1.32 |

| | | | | | | | | | | | | | | | |
|---|----------------|----------------|---------|------|---|-----|------|------|---|---|-------------------------------|---|-------|------|-------|
| PAC005_U2OS_6H:BRD-A71033472-003-04:9:10 | BRD-A71033472 | fendiline | 10 uM | 6 h | 2 | 16 | 0.05 | 0.03 | 1 | 0 | Calcium channel blocker | HTR2B | -0.36 | 0.48 | -1.32 |
| TAK004_U2OS_96H:TRCN0000006180:1 | TRCN0000006180 | PGK1 | 1 uL | 96 h | 3 | 107 | 0.23 | 0.16 | 0 | 0 | -666 | -666 | -0.36 | 0.49 | -1.32 |
| PAC004_U2OS_6H:BRD-K08356259-003-05:6:7.12159 | BRD-K08356259 | xylometazoline | 6.66 uM | 6 h | 2 | 48 | 0.18 | 0.09 | 1 | 1 | Adrenergic receptor agonist | ADRA2A ADRA2B ADRA2C ADRA1A ADRA1B ADRA1D | -0.35 | 0.46 | -1.31 |
| PAC002_U2OS_6H:BRD-K48722258-300-04:5:10 | BRD-K48722258 | dilazep | 10 uM | 6 h | 2 | 58 | 0.07 | 0.06 | 0 | 0 | Adenosine receptor antagonist | SLC29A1 CACNA1C | -0.35 | 0.46 | -1.31 |
| ASG003_U2OS_24H:M24 | BRD-K24681473 | YM-155 | 0.12 uM | 24 h | 5 | 616 | 0.62 | 0.63 | 1 | 1 | Survivin inhibitor | BIRC5 | -0.35 | 0.46 | -1.31 |

For Review Only

Supplementary File - Table 4. CMap targeted drug prediction results of genes from yellow model in U2OS cell line.

| ID | Perturbation identifier | Perturbation name | Perturbation dose | Perturbation time | Number of samples | Signature size in genes | Connectivity score at the 75th percentile | Treatment activity score | Quality control pass | High quality | Mechanism of action | Target name | Raw connectivity score | False discovery rate q-value | Normalized connectivity score |
|---|-------------------------|--------------------|-------------------|-------------------|-------------------|-------------------------|---|--------------------------|----------------------|--------------|---|--|------------------------|------------------------------|-------------------------------|
| TA.OE005_U2OS_72H:BRDN0000464873:1 | BRDN0000464873 | PPARGC1A | 1.0 uL | 72 h | 2 | 281 | 0.42 | 0.35 | 1 | 1 | -666 | -666 | -0.42 | 15.65 | -1.65 |
| MOA001_U2OS_24H:J03 | BRD-A18497530 | 5-iodotubercidin | 1.11 uM | 24 h | 3 | 415 | 0.64 | 0.52 | 1 | 1 | Adenosine kinase inhibitor | -666 | -0.38 | 2 | -1.5 |
| PAC001_U2OS_6H:BRD-K67298865-001-02-5:13.0077 | BRD-K67298865 | SB-431542 | 12.5 uM | 6 h | 2 | 143 | 0.24 | 0.19 | 0 | 0 | TGF-beta receptor inhibitor | TGFBR1 ACVR1C ACVR1B | -0.38 | 2.01 | -1.5 |
| TAK004_U2OS_96H:TRCN0000019807:1 | TRCN0000019807 | XBP1 | 1 uL | 96 h | 3 | 108 | 0.12 | 0.12 | 0 | 0 | -666 | -666 | -0.37 | 1.48 | -1.43 |
| PAC001_U2OS_6H:BRD-K65503129-001-01-4:10 | BRD-K65503129 | CCT-018159 | 10 uM | 6 h | 2 | 97 | 0.42 | 0.2 | 0 | 0 | HSP inhibitor | HSP90AA1 HSP90AB1 | -0.36 | 1.21 | -1.42 |
| TA.OE005_U2OS_72H:BRDN0000464922:1 | BRDN0000464922 | ATF4 | 1.0 uL | 72 h | 2 | 194 | 0.35 | 0.27 | 1 | 1 | -666 | -666 | -0.36 | 1.23 | -1.42 |
| LKCP002_U2OS_6H:H19 | BRD-K12742203 | moxaverine | 10 uM | 6 h | 4 | 117 | 0.2 | 0.16 | 1 | 1 | Phosphodiesterase inhibitor | -666 | -0.36 | 1.29 | -1.42 |
| PAC003_U2OS_6H:BRD-K28210218-236-04-0:10 | BRD-K28210218 | cephalothin | 10 uM | 6 h | 2 | 16 | 0.21 | 0.06 | 1 | 0 | Bacterial cell wall synthesis inhibitor | -666 | -0.36 | 1.35 | -1.42 |
| PAC004_U2OS_6H:BRD-K03842655-001-02-1:7.88393 | BRD-K03842655 | penitrem-a | 8 uM | 6 h | 2 | 221 | 0.56 | 0.36 | 1 | 1 | -666 | -666 | -0.36 | 1.08 | -1.41 |
| PAC001_U2OS_6H:BRD-K69023402-001-02-5:7.6834 | BRD-K69023402 | thapsigargin | 8 uM | 6 h | 2 | 471 | 0.72 | 0.59 | 0 | 0 | ATPase inhibitor | ATP2A1 | -0.36 | 1.08 | -1.4 |
| PAC003_U2OS_6H:BRD-A19500257-001-01-3:20 | BRD-A19500257 | geldanamycin | 20 uM | 6 h | 2 | 239 | 0.49 | 0.35 | 1 | 1 | -666 | -666 | -0.35 | 1.08 | -1.39 |
| PAC059_U2OS_6H:BRD-K10327449-001-01-7:10.1399 | BRD-K10327449 | SA-1457945 | 10 uM | 6 h | 3 | 234 | 0.42 | 0.32 | 1 | 1 | -666 | -666 | -0.36 | 1.08 | -1.39 |
| TAK004_U2OS_96H:TRCN0000154330:1 | TRCN0000154330 | SLIRP | 1 uL | 96 h | 3 | 164 | 0.31 | 0.23 | 0 | 0 | -666 | -666 | -0.36 | 1.08 | -1.39 |
| PAC005_U2OS_6H:BRD-A76746748-236-02-9:10 | BRD-A76746748 | cefuroxime | 10 uM | 6 h | 2 | 22 | 0.07 | 0.04 | 0 | 0 | Bacterial cell wall synthesis inhibitor | -666 | -0.35 | 1.04 | -1.38 |
| PAC002_U2OS_6H:BRD-K51751936-001-03-4:5.12147 | BRD-K51751936 | alfadolone-acetate | 4 uM | 6 h | 2 | 180 | 0.24 | 0.21 | 0 | 0 | GABA receptor agonist | -666 | -0.35 | 1.06 | -1.38 |
| PAC001_U2OS_6H:BRD-K69763916-001-01-7:10 | BRD-K69763916 | LY-341495 | 10 uM | 6 h | 2 | 245 | 0.35 | 0.3 | 0 | 0 | Glutamate receptor antagonist | GRM2 GRM3 | -0.35 | 1.03 | -1.37 |
| LKCP001_U2OS_24H:F17 | BRD-K49807096 | benazepril | 1.11 uM | 24 h | 5 | 95 | 0.25 | 0.15 | 0 | 0 | ACE inhibitor | ACE | -0.35 | 1.03 | -1.36 |
| PAC069_U2OS_6H:BRD-K59962020-001-09-3:20 | BRD-K59962020 | CHEMBL-374350 | 20 uM | 6 h | 3 | 318 | 0.52 | 0.41 | 1 | 1 | NFKB inhibitor | -666 | -0.35 | 1.03 | -1.36 |
| PAC001_U2OS_6H:BRD-K64245000-001-01-7:10 | BRD-K64245000 | GW-4064 | 10 uM | 6 h | 2 | 215 | 0.42 | 0.3 | 0 | 0 | -666 | -666 | -0.35 | 1.03 | -1.36 |
| LKCP002_U2OS_24H:O10 | BRD-K55026842 | azacitidine | 10 uM | 24 h | 5 | 454 | 0.56 | 0.51 | 0 | 0 | DNA methyltransferase inhibitor | DNMT1 DNMT3A | -0.34 | 1.03 | -1.35 |
| TAK004_U2OS_96H:TRCN0000033501:1 | TRCN0000033501 | BCL2L1 | 1 uL | 96 h | 3 | 98 | 0.23 | 0.15 | 0 | 0 | -666 | -666 | -0.35 | 1.03 | -1.35 |
| PAC003_U2OS_6H:BRD-K35430135-003-01-5:10 | BRD-K35430135 | SR-59230A | 10 uM | 6 h | 2 | 35 | 0.13 | 0.07 | 1 | 0 | Adrenergic receptor antagonist | ADRB3 ADRB1 ADRB2 | -0.34 | 1.03 | -1.34 |
| PAC059_U2OS_6H:BRD-K26676775-001-01-3:10.0654 | BRD-K26676775 | SA-1460192 | 10 uM | 6 h | 3 | 182 | 0.36 | 0.26 | 1 | 1 | -666 | -666 | -0.34 | 1.03 | -1.34 |
| PAC002_U2OS_6H:BRD-K49481516-004-03-5:10 | BRD-K49481516 | galantamine | 10 uM | 6 h | 2 | 185 | 0.48 | 0.3 | 0 | 0 | Acetylcholinesterase inhibitor | ACHE BCHE CHRNA1 CHRNA10 CHRNA2 CHRNA3 CHRNA4 CHRNA5 CHRNA6 CHRNA7 CHRNA9 CHRN B1 CHRN B2 CHRN B3 CHRN B4 CHRN D | -0.34 | 1.03 | -1.34 |

| | | | | | | | | | | | CHRNE CHRNG | | | | |
|---|---------------|-------------------------|---------|------|---|-----|------|------|---|---|--|---|-------|------|-------|
| PAC017_U2OS_6H:BRD-K34639619-001-01-1:10.0168 | BRD-K34639619 | SD-6-035-A1 | 10 uM | 6 h | 3 | 46 | 0.16 | 0.09 | 0 | 0 | -666 | -666 | -0.34 | 1.03 | -1.33 |
| PAC001_U2OS_6H:BRD-K62221994-001-01:8:10 | BRD-K62221994 | T-98475 | 10 uM | 6 h | 2 | 116 | 0.26 | 0.18 | 0 | 0 | Gonadotropin receptor antagonist | GNRHR | -0.34 | 1.03 | -1.33 |
| TAK004_U2OS_96H:TRCN000003161:1 | TRCN000003161 | RPS6KB1 | 1 uL | 96 h | 3 | 80 | 0.23 | 0.14 | 0 | 0 | -666 | -666 | -0.34 | 1.03 | -1.33 |
| PAC003_U2OS_6H:BRD-K24023109-001-02:5:12.0622 | BRD-K24023109 | diltiazem | 12 uM | 6 h | 2 | 81 | 0.1 | 0.09 | 1 | 0 | Calcium channel blocker | CACNA1C CYP3A5 CYP3A7 CACNA1S CACNA2D1 CACNG1 HTR3A KCNA5 | -0.34 | 1.03 | -1.32 |
| PAC002_U2OS_6H:BRD-K50417881-003-05:9:10 | BRD-K50417881 | etipendipine | 10 uM | 6 h | 2 | 104 | 0.32 | 0.18 | 0 | 0 | Dopamine receptor antagonist | DRD2 DRD3 DRD4 | -0.34 | 1.03 | -1.32 |
| PAC003_U2OS_6H:BRD-K31843556-001-01:7:10 | BRD-K31843556 | T-0070907 | 10 uM | 6 h | 2 | 244 | 0.2 | 0.22 | 1 | 1 | PPAR receptor antagonist | PPARG | -0.34 | 1.03 | -1.32 |
| PAC004_U2OS_6H:BRD-K14765469-003-02:3:6.76024 | BRD-K14765469 | vesamicol | 6.66 uM | 6 h | 2 | 36 | 0.24 | 0.09 | 0 | 0 | Acetylcholinesterase inhibitor | SLC18A3 | -0.33 | 1.03 | -1.31 |
| PAC003_U2OS_6H:BRD-K35960502-001-04:4:10 | BRD-K35960502 | niclosamide | 10 uM | 6 h | 2 | 145 | 0.52 | 0.28 | 1 | 1 | DNA inhibitor STAT inhibitor | STAT3 | -0.33 | 1.03 | -1.31 |
| PAC026_U2OS_6H:BRD-K18910433-001-18:4:20 | BRD-K18910433 | estradiol | 20 uM | 6 h | 3 | 179 | 0.47 | 0.29 | 1 | 1 | Estrogen receptor agonist | -666 | -0.33 | 1.03 | -1.3 |
| PAC001_U2OS_6H:BRD-K62240499-001-02:6:10 | BRD-K62240499 | huperzine-a | 10 uM | 6 h | 2 | 123 | 0.18 | 0.15 | 0 | 0 | Acetylcholinesterase inhibitor Glutamate receptor antagonist | ACHE | -0.33 | 1.03 | -1.3 |
| MOA001_U2OS_24H:M07 | BRD-K29313308 | HDAC3-selective | 10 uM | 24 h | 2 | 199 | 0.52 | 0.33 | 1 | 1 | HDAC inhibitor | -666 | -0.33 | 1.03 | -1.3 |
| PAC004_U2OS_6H:BRD-K15935639-001-02:0:9.06227 | BRD-K15935639 | z-leu3-VS | 10 uM | 6 h | 2 | 406 | 0.8 | 0.58 | 0 | 0 | Proteasome inhibitor | -666 | -0.33 | 1.03 | -1.3 |
| PAC003_U2OS_6H:BRD-K30867024-001-01:1:10 | BRD-K30867024 | SB-216641 | 10 uM | 6 h | 2 | 144 | 0.16 | 0.15 | 1 | 0 | Serotonin receptor antagonist | HTR1DI HTR1B HTR1A HTR2A HTR2B HTR2C | -0.33 | 1.03 | -1.29 |
| PAC059_U2OS_6H:BRD-K48945537-001-01:5:10.0054 | BRD-K48945537 | SA-1455791 | 10 uM | 6 h | 3 | 437 | 0.51 | 0.48 | 1 | 0 | -666 | -666 | -0.33 | 1.03 | -1.29 |
| PAC003_U2OS_6H:BRD-K36198571-001-01:2:10 | BRD-K36198571 | WAY-170523 | 10 uM | 6 h | 2 | 132 | 0.16 | 0.15 | 1 | 1 | Metalloproteinase inhibitor | MMP13 | -0.33 | 1.03 | -1.29 |
| LKCP002_U2OS_6H:D22 | BRD-K51318897 | fenbendazole | 10 uM | 6 h | 4 | 353 | 0.53 | 0.44 | 1 | 1 | Tubulin inhibitor | CYP2C19 CYP2D6 CYP2J2 CYP3A4 TUBB | -0.33 | 1.03 | -1.29 |
| LKCP002_U2OS_24H:P19 | BRD-K99749624 | linifanib | 10 uM | 24 h | 5 | 554 | 0.45 | 0.5 | 1 | 1 | PDGFR inhibitor VEGFR inhibitor | CSF1RKDR PDGFRB FLT1 FLT3 FLT4 PDGFRA CSF1KIT RET TEK | -0.33 | 1.01 | -1.28 |
| PAC003_U2OS_6H:BRD-K33818169-003-01:2:10 | BRD-K33818169 | GW-3965 | 10 uM | 6 h | 2 | 48 | 0.12 | 0.08 | 1 | 0 | LXR agonist ABC transporter expression enhancer | NR1H2 NR1H3 ABCA1 | -0.33 | 1.01 | -1.28 |
| PAC005_U2OS_6H:BRD-A52660433-066-01:3:10 | BRD-A52660433 | tetrindole | 10 uM | 6 h | 2 | 250 | 0.61 | 0.39 | 1 | 1 | Monoamine oxidase inhibitor | MAOA | -0.33 | 1.01 | -1.28 |
| PAC023_U2OS_6H:BRD-K45843042-001-01:3:9.85433 | BRD-K45843042 | SA-419083 | 10 uM | 6 h | 3 | 169 | 0.27 | 0.22 | 0 | 0 | -666 | -666 | -0.33 | 1.03 | -1.28 |
| PAC005_U2OS_6H:BRD-A55913614-316-04:7:10 | BRD-A55913614 | primaquine | 10 uM | 6 h | 2 | 91 | 0.04 | 0.06 | 1 | 0 | Antimalarial DNA inhibitor | KRT7 NQO2 | -0.32 | 1 | -1.27 |
| TA.OE005_U2OS_72H:BRDN000464855:1 | BRDN000464855 | CSNK1A1 | 1.0 uL | 72 h | 2 | 89 | 0.13 | 0.11 | 1 | 0 | -666 | -666 | -0.32 | 1 | -1.27 |
| PAC002_U2OS_6H:BRD-K56064827-001-04:7:14.7794 | BRD-K56064827 | EI-273 | 15 uM | 6 h | 2 | 97 | 0.24 | 0.15 | 0 | 0 | PKC inhibitor | PRKCA PRKCG | -0.32 | 1 | -1.27 |
| TA.OE005_U2OS_72H:BRDN000404346:1 | BRDN000404346 | RPTOR | 1.0 uL | 72 h | 2 | 362 | 0.02 | 0.09 | 0 | 0 | -666 | -666 | -0.33 | 1 | -1.27 |
| PAC002_U2OS_6H:BRD-K45662124-001-01:8:10 | BRD-K45662124 | 3'-fluorobenzylpiperone | 10 uM | 6 h | 2 | 221 | 0.6 | 0.37 | 0 | 0 | Dopamine receptor antagonist | -666 | -0.32 | 0.94 | -1.26 |

| | | | | | | | | | | | | | | | |
|--|---------------|--------|-------|-----|---|-----|------|------|---|---|----------------------------|-------|-------|------|-------|
| PAC002_U2OS_6H:BRD-K45479396-001-01:8:10 | BRD-K45479396 | BP-554 | 10 uM | 6 h | 2 | 253 | 0.46 | 0.34 | 0 | 0 | Serotonin receptor agonist | HTR1A | -0.32 | 0.94 | -1.26 |
|--|---------------|--------|-------|-----|---|-----|------|------|---|---|----------------------------|-------|-------|------|-------|

For Review Only